MODELING GROUND ELEVATION OF LOUISIANA COASTAL WETLANDS AND ANALYZING RELATIVE SEA LEVEL RISE INUNDATION USING RSET-MH AND LIDAR MEASUREMENTS

by

Jing Liu

A Dissertation Submitted to the Faculty of

The Charles E. Schmidt College of Science

In Partial Fulfillment of the Requirements for the Degree of

Doctor of Philosophy

Florida Atlantic University

Boca Raton, FL

August 2020

MODELING GROUND ELEVATION OF LOUISIANA COASTAL WETLANDS AND ANALYZING RELATIVE SEA LEVEL RISE INUNDATION USING RSET-MH AND LIDAR MEASUREMENTS

by

Jing Liu

This dissertation was prepared under the direction of the candidate's dissertation advisor, Dr. Caiyun Zhang, Department of Geosciences, and has been approved by the members of her supervisory committee. It was submitted to the faculty of the Charles E. Schmidt College of Science and was accepted in partial fulfillment of the requirements for the degree of Doctor of Philosophy.

SUPERVISORY COMMITTEE:

Caiyun Zhang, Ph.D.
Dissertation Advisor

Diana Mitsova-Boneva (Jul 28, 2020 20:53 EDT)

Diana Mitsova, Ph.D.

Tobin Hindle, Ph.D.

Mingshun Jiang (Aug 11, 2020 10:35 EDT)

Mingshun Jiang, Ph.D.

Zhixiao Xie, Ph.D.
Chair, Department of Geosciences

Ata Sarajedini, Ph.D.
Dean, The Charles E. Schmidt College of Science

Robert W. Stackman Jr., Ph.D.
Dean, Graduate College

August 12, 2020

Date

ACKNOWLEDGMENTS

This dissertation work was made possible through help from the Coastal Protection and Restoration Authority.

Many thanks to my advisor Dr. Caiyun Zhang, my committee members Dr. Diana Mitsova, Dr. Tobin Hindle, and Dr. Mingshun Jiang, and my friends and family for all their support.

ABSTRACT

Author: Jing Liu

Title: Modeling Ground Elevation of Louisiana Coastal Wetlands and Analyzing Relative Sea Level Rise Inundation Using RSET-MH and LiDAR Measurements

Institution: Florida Atlantic University

Degree: Doctor of Philosophy

Dissertation Advisor: Dr. Caiyun Zhang

Year: 2020

The Louisiana coastal ecosystem is experiencing increasing threats from human flood control construction, sea-level rise (SLR), and subsidence. Louisiana lost about 4,833 km^2 of coastal wetlands from 1932 to 2016, and concern exists whether remaining wetlands will persist while facing the highest rate of relative sea-level rise (RSLR) in the world. Restoration aimed at rehabilitating the ongoing and future disturbances is currently underway through the implementation of the Coastal Wetlands Planning Protection and Restoration Act of 1990 (CWPPRA). To effectively monitor the progress of projects in CWPPRA, the Coastwide Reference Monitoring System (CRMS) was established in 2006. To date, more than a decade of valuable coastal, environmental, and ground elevation data have been collected and archived. This dataset offers a unique opportunity to evaluate the wetland ground elevation dynamics by linking the Rod Surface Elevation Table (RSET) measurements with environmental variables like water salinity and biophysical variables like canopy coverage. This dissertation research

examined the effects of the environmental and biophysical variables on wetland terrain elevation by developing innovative machine learning based models to quantify the contribution of each factor using the CRMS collected dataset. Three modern machine learning algorithms, including Random Forest (RF), Support Vector Machine (SVM), and Artificial Neural Network (ANN), were assessed and cross-compared with the commonly used Multiple Linear Regression (MLR). The results showed that RF had the best performance in modeling ground elevation with Root Mean Square Error (RMSE) of 10.8 cm and coefficient of coefficient (r) = 0.74. The top four factors contributing to ground elevation are the distance from monitoring station to closest water source, water salinity, water elevation, and dominant vegetation height.

Collecting terrain elevation measurements using modern Light Detection and Ranging (LiDAR) remote sensing is challenging in wetlands with thick vegetation, and LiDAR derived Digital Elevation Models (DEM) in wetlands are often highly uncertain. This dissertation, for the first time, examined the potential of improving LiDAR DEM using RSET data at the regional scale by developing an object-based machine learning correction approach. A comparison of RF, SVM, ANN, and MLR algorithms revealed that RF was the best approach for LiDAR DEM correction with a correlation coefficient (r) of 0.83 and RMSE of 8 cm.

Finally, the inundation of coastal Louisiana in 2050 was predicted by using the corrected 2017 LiDAR DEM and annually increased by ground elevation change to 2050. Both object-based and grid-based inundation maps were produced and compared, which revealed that, based on the current RSLR rate, 34% of the selected area would be inundated by 2050.

DEDICATION

This dissertation is dedicated to my parents Yingjie Liu and Cuifen Feng, and my husband Salvatore John Calise. All this work could not have been completed without their unconditional love and support.

MODELING GROUND ELEVATION OF LOUISIANA COASTAL WETLANDS AND ANALYZING RELATIVE SEA LEVEL RISE INUNDATION USING RSET-MH AND LIDAR MEASUREMENTS

LIST OF TABLES

LIST OF FIGURES

ABBREVIATIONS

ANN	Artificial Neural Network
CWPPRA	Coastal Wetlands Planning, Protection and Restoration Act
CRMS	Coastwide Reference Monitoring System
LiDAR	Light Detection and Ranging
MAE	Mean Absolute Error
MLR	Multiple Linear Regression
NAVD 88	North American Vertical Datum of 1988
RSLR	Relative Sea-Level Rise
RSET-MH	Rod Surface-Elevation and Mark Horizon
RMSE	Root Mean Squared Error
R^2	Coefficient of Determination
RF	Random Forest
r	Pearson's Correlation Coefficient
SLR	Sea-level Rise
SVM	Support Vector Machine

CHAPTER 1: INTRODUCTION

1.1 Louisiana coastal wetland ecosystems and restoration

The Louisiana coastal zone encompasses approximately 37,780 square kilometers, including the Mississippi Deltaic Plain to the east and the Chenier Plain to the west formed by dynamic interactions between the Mississippi River and the coast (Boesch et al., 1994). As glaciers retreated and meltwater inundated lands and periodic floodwater carried sedimentary material to the lower floodplains, forming a vast expanse of coastal wetlands (Fisk and McFarlan, 1955). Hydrology was keep dictating the vegetation distribution parallel to the coast, representing graduation from high salinity tolerated saltmarsh near the coast to brackish marshes, then to inland freshwater marshes and wooded swamps (Boesch et al., 1994).

Coastal Louisiana wetlands are critical environments because they provide treasured ecosystem services, including improved water quality, food production, carbon sequestration, wildlife habitats, habitats for commercial fisheries, and storm-related disturbance regulation (Costanza et al., 2014). However, coastal Louisiana wetlands are also one of the most threatened environments, currently experiencing more significant land loss than all other states within the U.S. due to multiple compounding and interacting stressors (Couvillion et al., 2017). The highly dynamic coastal wetlands environment in Louisiana has dramatically grown and retreated depending on the wetland ground elevation and changes in sea level (Boesch et al., 1994). With the high rate of subsidence associated with global rising sea levels, coastal wetlands in Louisiana are experiencing the highest relative sea-level rise (RSLR) in the world at 12 ± 8.3 mm per year (Jankowski et al., 2017). Increasingly rising sea levels have resulted in large areas of brackish and freshwater wetlands becoming progressively more saline, as saltwater has increasingly invaded the deteriorating coastal area of Louisiana (Boesch et al., 1994). Additionally, the decreased sediment supply by river leveeing and damming (Blum & Roberts, 2009) and dredging of navigation canals (Day et al., 2000) along the Mississippi River have eliminated freshwater and sediment input to coastal zones. These flood control structures have caused sediment deprivation and have contributed to reduced capacity for sediment accretion, thereby reducing the ability of wetlands to maintain ground elevation in response to RSLR (Couvillion et al., 2017). As a result, coastal Louisiana has lost about 4,833 square kilometers of land from 1932 to 2016 (Couvillion et al., 2017).

Growing awareness of rapid coastal wetland loss has resulted in extensive studies (e.g., Kolker et al., 2011; Blum & Roberts, 2009; Syvitski, 2008; Day et al., 2007; Day et al., 2000), and state and federal statutes have been enacted that authorize and finance coastal restoration on a large regional scale. Several policies have been implemented in response to this massive land loss in coastal Louisiana. The Coastal Wetlands Planning, Protection and Restoration Act of 1990 (CWPPRA) was enacted to create, restore, enhance, and protect coastal wetlands in Louisiana. Subsequently, the Coastwide Reference Monitoring System (CRMS) was developed to collectively assess the effectiveness of restoration projects carried out under the CWPPRA, by providing an array of reference sites for a scientific evaluation network to achieve statistically valid comparisons (Steyer et al., 2003). The 392 CRMS monitoring stations were randomly selected and allocated to major coastal wetland types, including fresh intermediate, brackish, saline, and swamp, and established between 2006 and 2008 (Figure 1.1) (Folse et al., 2018). At each CRMS monitoring station, sediment elevation, vertical accretion, hydrologic data, and vegetation data are collected through a partnership of the United States Geological Survey and Coastal Protection and Restoration Authority (CPRA).

Sediment elevation is measured by the Rod Surface Elevation Table – Mark Horizon (RSET-MH) method (Cahoon et al., 2002), which provides a highly precise (with ±1.3 mm vertical accuracy) and repeatable approach used to collect relative cumulative sediment change data in 6-month intervals from 2007 to the present. The RSET produces the most precise and easily replicable measurements for local sediment elevation (Cahoon et al., 2002; Webb et al., 2013). While the RSET method is a nondestructive process that precisely measures sediment elevation in coastal wetlands, it is limited by high labor cost and accessibility of the site (Webb et al., 2013; Scott & Hensel, 2007) . Additionally, the limited number and low density of CRMS monitoring stations makes scaling up and mapping broader regional scale sediment elevation changes a challenge (Webb et al., 2013). In general, the field method for monitoring sediment elevation is costly and time-consuming; therefore, techniques that enhance confidence in assessing restoration status with higher spatial coverage across the entire coastal zone of Louisiana are in high demand for managers, especially as wetland restoration efforts increase to mitigate the impacts of the high rate of RSLR (Webb et al., 2013).

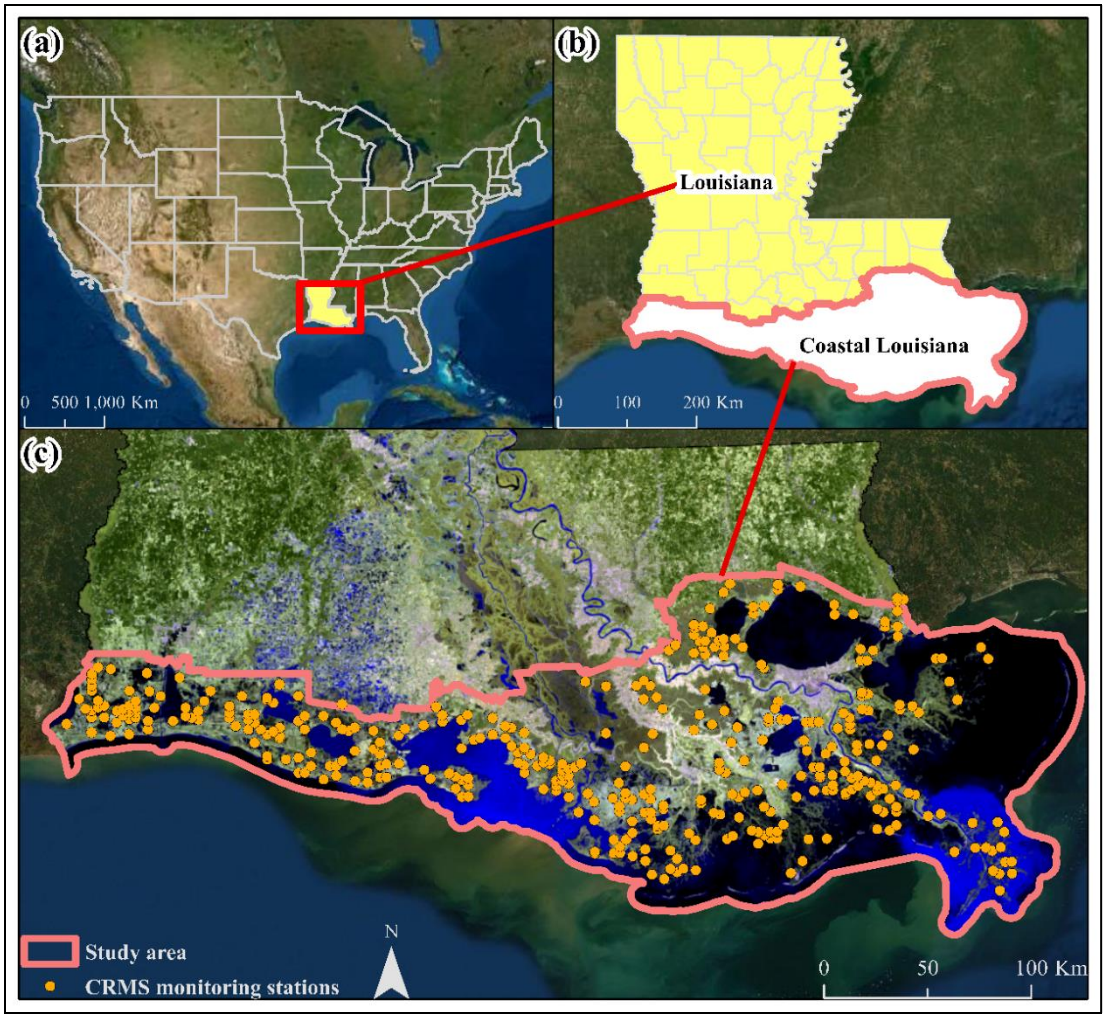

Figure 1.1 Location of the state of Louisiana, USA (a); location of the study area in coastal Louisiana (b); and distribution of CRMS monitoring stations (c).

1.2 LiDAR remote sensing and its limitation for DEM generation in wetlands

Unlike the field-based techniques for estimating sediment elevation, remote sensing has revolutionized the ability to map and model larger scale environments and has contributed greatly to generating high-density regional-scale ground elevation maps. Airborne Light Detection and Ranging (LiDAR) is an active remote sensing technology that can provide high-resolution topographic information by emitting infrared signals directed at the ground, which hit objects and are reflected back to a sensor on the aircraft.

The time elapsed between signal emission and the arrival of the reflection of that signal at the sensor allows the computation of elevation and height information (McClure et al., 2016). Compared to low-density point scale field measuring sites along the coastal zone of Louisiana, LiDAR systems with a point density of 1 point per square meter are commonly available, and systems with 8 to 10 points per square meter are becoming the norm with technology advancements (Hladik and Alber, 2012). LiDAR technologies acquire 3-dimensional coordinates of objects and provide unprecedentedly detailed point-cloud topography descriptions over large areas (Wang et al., 2009).

Discrete LiDAR signal returns allow discrimination of multiple laser hits; the first return often originates from reflection off the top of the object, while the last returns are assumed to be from the ground (Hladik and Alber, 2012). LiDAR last returns have been recognized as a standard to generate high spatial resolution Digital Elevation Models (DEM) to represent bare earth elevation (Kulawardhana et al., 2014; Lefsky et al., 2002). The DEM is the collection of square pixels where the pixel value is the LiDAR last return elevation. Many studies have shown that the DEM accuracy depends on the land cover types, terrain characteristics, interpolation methods, LiDAR point density, and LiDAR filtering methods (e.g., Fisher and Tate, 2006; Li et al.,2005; Liu et al., 2008).

Although LiDAR-derived DEM has shown great success in representing some environments (Montané and Torres, 2006), little progress has been reported in LiDAR applications for the characterization of relatively short and high-density herbaceous vegetation coastal wetlands. LiDAR is challenging for monitoring ground elevation in wetland environments for two main reasons. First, high-density vegetation leads to a relatively low chance for LiDAR lasers to penetrate through the vegetative canopy layer and hit the ground (Marani et al., 2004). Instead of hitting the ground, laser signals might hit the vegetation surface then return to the LiDAR receiver as a "ground" return (Rosso et al., 2006). Moreover, the true laser ground returns are challenging to separate from the laser signals that hit the vegetation surface. Consequently, LiDAR tends to overestimate coastal wetland ground elevation (Montané and Torres, 2006; Rosso et al., 2006; Schmid et al., 2011). Second, the relatively short marsh vegetation is usually less than 2 m tall in coastal wetlands, which is similar to LiDAR pulse separation, which varies from 0.5 to 10 ns apart and correlates to 0.1 to 1.5 m pulse length. The distance between laser returns from the vegetation and the ground can be less than the pulse length, which will challenge the LiDAR system to reconcile as separate returns (Hopkinson et al., 2005). Thus, even when a last return LiDAR signal is correctly identified, it may not have originated from the actual ground, instead coming off short vegetation (Göpfert et al., 2006). As a result, the identified LiDAR last could not provide accurate information on the ground information and could not be used to directly determine the elevation of the ground (Wang et al., 2009).

Due to high-density vegetation, only 2-3% of LiDAR lasers penetrate through the vegetation canopy to hit the ground, then return and record as ground elevation (Wang et al., 2009). The vertical error in LiDAR-derived DEM urban area ranges from 0.10 m to 0.20 m, in high-density vegetation, the vertical error can be up to 0.31 m (Hladik and Alber, 2012; Montané and Torres, 2006; Hodgson et al., 2004). For local to regional scale RSLR inundation mapping, the National Oceanographic and Atmospheric Association (NOAA) recommends that the vertical error of a DEM should be at least twice as certain as the RSLR increment, which is difficult to achieve with available public LiDAR

(NOAA, 2010). Uncorrected DEM cannot meet the accuracy requirements to distinguish topographic changes in coastal wetlands at the resolution for RSLR inundation mapping (Hladik and Alber, 2012).

There have been several approaches developed in recent years to improve accuracies of LiDAR-derived DEM, including minimum bin gridding, which assumes the lowest LiDAR point value in the grid is the ground elevation (Medeiros et al., 2015; Schmid et al., 2011; Wang et al., 2009; Töyrä et al., 2003). Additionally, since LiDAR DEM were shown to overestimate ground elevation, subtraction of vegetation species-specific bias was applied for improving DEM accuracy (e.g., Hladik and Alber, 2012; Hladik et al., 2013; McClure et al., 2016). Finally, the fusion of airborne LiDAR with multi-spectral imagery using object-based correction has shown promise for increasing vertical accuracy of LiDAR-derived DEM (e.g., Cooper et al., 2019). I discuss these approaches in further detail in Section 3.1.2.

1.3 Machine learning based models for ground elevation and correction in wetlands

Artificial intelligence or machine learning has produced several powerful algorithms that have demonstrated immense potential in increasing understanding of environmental variables' impact on ground elevation and correcting LiDAR derived DEM. Machine learning approaches are often preferred in remote sensing problems due to the complicated and relationships between dependent and independent variables in wetlands ecosystem (Roger et al., 2018). Unlike traditional statistical analysis that utilizes Multiple Linear Regression (MLR) techniques to make predictions of the variable outcome, nonparametric modeling does not require the data be normally distributed (Bourennane et al., 2014). There are numerous machine-learning algorithms available, this study examined three machine learning algorithms for analyzing the relationship between environmental variables impact on ground elevation and LiDAR correction including Random Forest (RF), Support Vector Machine (SVM), and Artificial Neural Network (ANN) compete with MLR (Table 1.1).

RF is a decision tree classifier with many single decision trees using a majority vote of all trees for a more accurate prediction (Breiman, 2001). RF model builds from randomly and recursively split the input data depending on an if-then threshold, which results in a wide variety of trees (Pal and Mather, 2003). It is robust to parameter settings, limited training samples, and uncertain data quality (Maxwell et al., 2018). Another benefit is that overfitting could be avoided by reducing the number of decision trees and reducing the number of variables for each node, which would reduce the accuracy in the training data but generally increase the accuracy of testing unknown data (Pal and Mather, 2003). SVM is a supervised non-parametric statistical learning technique that aims to find the optimal boundary to separate classes based on the training samples then to separate simulation data under the same configurations (Mountrakis et al., 2011). These optimal boundaries can be linear or using kernel functions for a higher dimension (Huang et al., 2002). Furthermore, SVM typically applies one-against-all, one-against-others as workarounds for multi-class problems (Mountrakis et al., 2011). Thus, SVM-based classification has been known to balance accuracy attained with a finite amount of training data and the ability to generalized apply on unseen data (Mountrakis et al., 2011).

On the other hand, ANN is a learning technique designed to simulate neuron networks of the human brain (Mas and Flores, 2008). Specifically, the ANN system is formed from hundreds of processing elements as artificial neurons and is organized into layers, where all the neurons within a layer are connected to all the neurons in adjacent layers with relative weights (Agatonovic-Kustrin and Beresford, 2000). The weights are randomly guessed during training with iteratively adjusting and observing the effect on output nodes. The adjustments which improve the classification are kept and reinforced while adjustment that does not is discarded. Until the errors in the predictions are minimized, the inter-unit connections are optimized and ready for application on new data to predict the output (Agatonovic-Kustrin and Beresford, 2000). These three machine learning algorithms have shown good performance in analyzing non-linear regression in wetland ecosystems and show improvement over standard parametric methods (Zhang and Xie, 2014; Zhang et al., 2018; Zhang et al., 2019).

1.4 Significance of this dissertation

Coastal Louisiana has lost about 4,833 km^2 of wetlands over the past century, and concern exists whether remaining land will persist while facing the highest rates of RSLR in the world (Jankowski et al., 2017). The resilience of coastal wetlands is influenced by several environment variables, and for wetlands to persist, ground elevation must be gained at a rate that equals or exceeds the rate of RSLR (Rogers et al., 2012). Increasing our knowledge of how environmental variables impact ground elevation is crucial for modeling the response of coastal wetlands to rising sea levels. However, previous studies on the relationship between environmental variables and sediment ground elevation have primarily focused either on qualitative analysis (e.g., Krauss et al., 2008) or linear modeling techniques (e.g., Rogers et al., 2012). Due to the complicated processes involved in sediment elevation in the wetland ecosystem, there is a potential for a machine learning algorithm to analyze the non-linear relationship between ground elevation and environmental variables.

Fusing high vertical accuracy in-situ ground elevation data with a remote sensing dataset provides an opportunity for higher spatial coverage to enhance the confidence in assessing restoration status in coastal wetlands. With the broader spatial distribution and high vertical accuracy of ground elevation measured by RSET, there is a potential for better enhancement of LiDAR-derived DEM performance in Louisiana coastal wetlands. Meanwhile, instead of LiDAR-derived DEM traditionally corrected at the pixel level, Object-based Image Analysis (OBIA) incorporates similar pixels into a homogeneous image object, which represents a more ecologically relevant landscape unit. This dissertation research is the first application using the fusion of field-based ground elevation data derived from RSET techniques to calibrate and supplement LiDAR-acquired elevation data during DEM generation at an image object level. The restoration of coastal wetlands in Louisiana will benefit from the development of a robust methodology for mapping and assessing the potential impacts of future RSLR on a regional landscape scale.

1.5 Research objectives

The main objective of this dissertation research is to develop machine learning based models to quantify wetland ground elevation using relevant environmental variables and improve LiDAR-derived DEM using RSET-MH data, which will assist with wetland conservation, preservation, and restoration in the coastal Louisiana area. To achieve this overall goal, this dissertation was divided into three separate projects. The specific objectives of the three projects were:

1. Develop a time-series sediment surface elevation model to quantify the impact of environmental variables on wetland ground elevation dynamics.
2. Explore a data fusion technique by combining RSET-MH data, LiDAR DEM data, and aerial photography to improve LiDAR DEM.
3. Predict coastal inundation in 2050 due to RSLR using object-based RF corrected LiDAR-derived DEM and RSET-MH derived elevation change rate.

Table 1.1 Linear regression and machine learning algorithms.

Model	Description	Pros	Cons	References
Multiple linear regression (MLR)	MLR attempts to model the relationship between two or more explanatory variables and a response variable by fitting a linear equation to observed data	Ability to determine the relative influence of one or more predictor variables to the criterion value and ability to identify outliers	Limited by linear relationship and requirement of normally distributed data	Eberly, (2007)
Random forest (RF)	RF is an ensemble of many decision trees that are not influenced by each other	Ability to spot outliers/anomalies; discovering data patterns; identifying important predictors; predicting future outcomes.	Produces somewhat more accurate classification models than regression	Breiman, (2001)
Support vector machines (SVM)	SVM finds a hyperplane to separate the dataset into a discrete predefined class consistent with the training samples	Balance between accuracy obtained from small training data and the ability to generalize to unseen data and avoid overfitting	Challenge to choose kernel function to provide optimal SVM configuration	Mountrakis et al., (2011)
Artificial neural network (ANN)	ANN is a parameterized system designed to simulate how the human brain processes information	Ability to learn and model non-linear and complex relationships, with no restrictions on the input variables	ANN requires large training sets and is complicated	Agatonovic-Kustrin & Beresford, (2000)

CHAPTER 2: MODELING COASTAL WETLAND GROUND ELEVATION USING ENVIRONMENTAL VARIABLES

2.1 Introduction

Coastal wetlands, including marshes and swamps in Louisiana, occur at the interface of land and ocean, and are covered by emergent vegetation and regularly flooded. Wetland ecosystems are ecologically crucial components of the coastal landscape since they perform many critical ecosystem functions, such as storm surge buffering and carbon sequestration, and provide essential habitats for wildlife (Barbier et al., 2011). The long-term survival of the wetlands depends on their ability to build vertically at rates higher than relative sea-level change or else migrate inland at a rate faster than erosion at their seaward boundary (Morris et al., 2002; Kirwan et al., 2016). In the vertical dimension, coastal wetlands maintain their elevation by mineral sediment deposition from tide or river (Leonard and Luther, 1995) and through organic matter accumulation from vegetation (Nyman et al., 2006). With low initial ground elevation and a relatively high subsidence rate, the ground elevation is crucial for coastal Louisiana.

2.1.1 Environmental drivers impact the ground elevation

External forces like sea level, storms, and variations in sediment supply by human activities can strongly affect evolution of the coastal wetlands and influence the coupling between sediment deposition and organic matter accumulation (Mariotti and Fagherazzi, 2010). Modest stress from environmental drivers may spur trapping of sediment, plant productivity (Morris et al., 2002), and organic matter accumulation (Fagherazzi et al., 2012). However, with low initial ground elevation and relatively high subsidence rate in the coastal wetlands of Louisiana, the vertical accretion can be partially or entirely offset by stress from environmental drivers (Jankowski et al., 2017; Kirwan and Guntenspergen, 2012). Ground elevation processes operate in response to a range of environmental drivers, including sea-level rise (SLR), storms, and the human factor, as shown in Figure 2.1.

Coastal wetlands are inextricably linked to sea level because flooding is the primary mechanism for sediment delivery to the wetland platform (Fagherazzi et al., 2012). Tidal flooding promotes the transport of suspended sediments in tidal currents to the wetland platform, where they may be deposited. Explicitly, increased tidal frequency and inundation duration caused by SLR tends to increase mineral deposition rates (Cadol et al., 2014; Cahoon, 1995; Friedrichs and Perry, 2001; Leonard, 1997). Studies have found that wetlands that are inundated for long periods of time have a higher mineral deposition rate than wetlands that are periodically flooded (e.g., Bricker-Urso et al., 1989; Cahoon, 1995). Therefore, mineral deposition rates are strongly correlated to SLR accompanied by extensive flooding duration and frequency. Additionally, sediment accumulation is generally regarded to be inversely proportional to the distance from the sediment source, including rivers and coastal lines (Rogers et al., 2015). Studies have shown the distance of the site from the nearest source of tidal water or river impacts vertical accretion (Chmura and Hung, 2004). At sites closer to the sediment source (main channel or shoreline), the higher suspended inorganic sediment can be loaded and deposited at especially high rates (Kirwan and Murray, 2007).

Similar to SLR, storms have long been recognized as strong geomorphological drivers for ground elevation. Large amounts of resuspended sediments deposited by storms contribute significantly to vertical accretion (Day et al., 2007). Massive storm energy provides the opportunity for sediments from the ocean bed to be raised, suspended, and transported across the coastal landscape, then stored as wave energy is reduced. Up to 68 g/cm^2 of sediment were deposited on Louisiana coastal wetlands during Hurricane Katrina (Turner et al., 2006). Although storm surge can bring massive mineral and organic matter sediment deposits, colossal storm tides also lead to soil volume compaction, erosion, sediment redistribution, and seawater intrusion, resulting in overall ground elevation loss (Cahoon, 2006). In particular, Hurricane Katrina and Rita in 2005 eroded 527 km^2 of wetlands within the Louisiana coastal plain (Howes et al., 2010).

In addition to SLR and storms as environmental drivers, the coastal wetlands in Louisiana have been extensively modified by humanmade engineering structures that alter the timing and amount of river flow, such as levee banks, floodgates, and canals (Day et al., 2007; Rogers et al., 2015). Flood mitigation construction results in declining river inputs and insufficient sediment deposition from rivers to the coast (Day et al., 2000). For example, the sediment load of the Mississippi River has decreased 50% due to flood construction (Blum and Robbers, 2009). The success of ground elevation building depends on the balance between sediment supply and accommodation by SLR (Blum and Robbers). However, the modern sediment supply load is reduced, and sediment storage is insufficient for building ground elevation compared when factoring in increasing SLR, causing large-scale coastal wetland loss in the Mississippi Delta (Day et al., 2007).

Ground elevation change is positively correlated with vegetation biomass due to trapping of mineral and organic particles previously suspended in the water column (e.g., Nyman et al., 2006; Morris et al., 2002). Vegetation biomass includes vegetation, living roots, and rhizomes that exert significant friction on flowing water, attenuating the velocity of tidal flow and waves and enhancing the trapping and binding of mineral sediment and organic materials, promoting increased ground elevation (Mudd et al., 2010; Rogers et al., 2015). Laboratory experiments from Palmer et al. (2004) determined that sediment particle capture is a function of the density and diameter of the stem, sediment diameter, water flow velocity, suspended sediment concentration, and flow depth. With sufficient sediment supply, plant rooting activities can consolidate the sedimented clays and silts to form a plateau (Fagherazzi et al., 2012). In addition to dense vegetation, the canopy enhances sediment deposition; organic matter accounts for more than 40% of the total vertical accretion rate in Louisiana (Nyman et al., 2006). Surface plant litter and dead vegetation remaining after decomposition contribute to soil volume and to building ground elevation in coastal wetlands (Rogers et al., 2015).

Increased flood frequency and duration from SLR affect the colonization, production, and mortality of coastal wetland vegetation when water inundation surpasses the plant survival threshold. Coastal vegetation develops in intertidal zones when conditions allow for sufficient plant growth. However, water level increases make it difficult for new vegetation to establish on the tidal flat (Mariotti et al., 2010). Increased flooding frequency causes seedlings to fail to develop sufficient roots for anchoring to withstand the drag force from tide waves (Friess et al., 2012). Besides vegetation colonization, negative feedback between plant growth and increased flood depth caused by SLR has been analyzed (e.g., Morris et al., 2002). Plants are most productive at an optimum elevation with the mean high tide. When wetland ground elevation is lower than the optimum elevation, and increased flooding depth during tide leads to a decrease in plant productivity, this results in a decrease in building ground elevation. Increased SLR leads to the drowning of coastal wetlands vegetation and the marsh may ultimately become too deep for plants to survive (Marani et al., 2007a). Eventually, when the sea level consistently exceeds the threshold of submergence duration for vegetation survival, it will gradually cause plant mortality as well as convert emergent vegetation into intertidal mudflats or open water. Large-scale vegetation absence leads to rapid loss of ground elevation, thus further precluding the vegetation return and causing wetland edge erosion, peat collapse (Fagherazzi et al., 2012; Temmerman et al., 2012).

As a coastal buffer, wetlands vegetation reduces the height and erosion power of severe waves from storm surges propagating inland, which causes sediment erosion and reduces ground elevation on the coastal line (Gedan et al., 2011). The storm surge brought by Hurricanes Katrina and Rita eroded 527 km2 of wetlands in Louisiana plain (Howes et al., 2010). Coastal wetlands experience different types of damage from storm surge, including vegetation mortality high tide wrack, salt intrusion, and wetland edges erosion (Feagin et al., 2009), as well as the removal of bulk sediments from the vegetation mat (Howes et al., 2010). High and low salinity vegetation regimes present different erosion rates after storm surge. Impact studies of Hurricanes Katrina and Rita found that low salinity wetlands were preferentially eroded, while higher salinity wetlands were mainly unchanged (Howes et al., 2010). The extent of these damages affected recovery time and the health of the coastal wetlands and may lead to permanent wetland loss (Day et al., 2007).

In addition to SLR and storm environmental drivers, human activities have extensively modified and altered the structure and function of the ecosystem in the coastal wetlands of Louisiana. In particular, engineering construction, such as ditches and dikes, promote soil drainage to mitigate flooding and inundation for converting wetlands into agricultural land (Rogers and Woodroffe, 2015). As a result, sulphate-rich soils in coastal wetlands that oxidize as a result of drainage can cause significant soil acidification, and acid drainage can impact the health of vegetation. Moreover, altered inundation by ditches breaks anaerobic soil conditions and leads to air exposure, which causes organic-rich soil to be oxidized and results in significant soil compaction and loss of ground elevation (Rogers & Woodroffe, 2015).

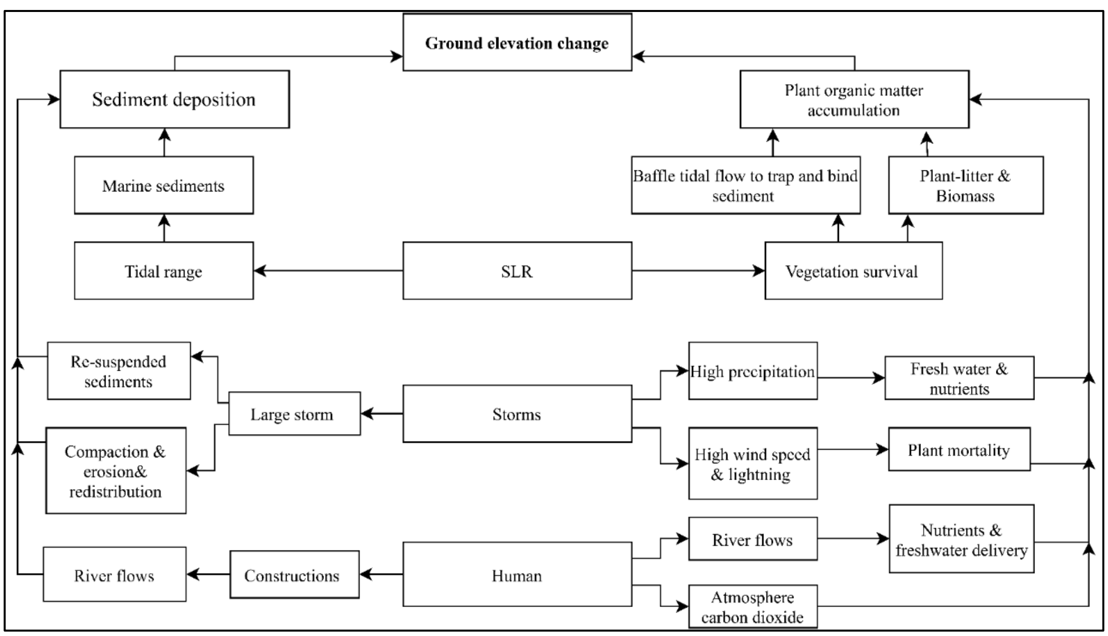

Figure 2.1 A conceptual diagram illustrating how environmental drivers and accretion processes influence coastal wetland ground elevation development. Adapted from Cahoon et al., 2009.

2.1.2 Significance of modeling ground elevation using environmental variables

Models of ground elevation dynamics have been popularly used for monitoring and modeling coastal wetland vulnerability to SLR around the world (e.g. Morris et al., 2002; Rogers et al., 2012; Stagg et al., 2013; Schile et al., 2014). Morris et al. (2002) developed a mechanistic numerical model: the Marsh Equilibrium Model (MEM) incorporates physical inputs (initial rate of sea level, sediment concentration, and starting marsh elevation) and biotic inputs (height of marshes, aboveground biomass, and biomass decay rate) to model ground elevation. In coastal Australia, Rogers et al. (2012) generated MLR empirical models of estuary wetland sediment accretion incorporating time, elevation, distance to the channel, 6-month average monthly maximum water level, and 6-month average monthly rainfall (Rogers et al., 2012). Subsequent efforts by Stagg et al. (2013) in coastal Louisiana integrated five years of Rod Surface Elevation Table (RSET) data with local relative water-level trends using simple linear regression to create a submergence vulnerability index (SVI), which assesses the vulnerability of each Coastwide Reference Monitoring System (CRMS) site to submergence. Based on projected ground elevation, projected SLR, and frequency of flooding, SVI scores were allocated to a site to indicate the vulnerability to submergence (Stagg et al., 2013).

However, since coastal wetlands are located in intertidal environments, the process of quantifying ground elevation is a complicated function resulting from a range of continental and regional scale environmental variables (Cahoon, 2006). Additionally, the relationship between ground elevation and environmental drivers is often non-linear (Jankowski et al., 2017). Simply assuming a linear relationship between dependent variables (ground elevation) and independent variables (environmental drivers) in coastal wetlands would result in high uncertainty during SLR vulnerability assessments. Moreover, a large-scale quantitative assessment of how environmental drivers impact ground elevation in coastal wetlands is needed. Specifically, the same process (e.g., sedimentation) impacted by a small-scale environmental driver may be governed by a different environmental variable at a large scale (Friess et al., 2012).

Upstream flood control constructions, including levee and damming construction and river damming, have reduced terrestrial sediment input into the coastal zone in Louisiana (Coleman et al., 1998). Furthermore, with rising sea levels and subsidence causing vertical accretion deficits in coastal wetlands and widespread land loss throughout the modern delta region, a comprehensive landscape vulnerability analysis is necessary for coastal management and to provide a guideline for coastal wetlands scientists (DeLaune et al., 1989; Kesel, 1988). Ground elevation is crucial for coastal wetland survival. It is important to use an ecosystem-based model of a large area to study the spatial interactions and mechanisms among different environmental drivers that impact ground elevation. The data were derived from the public data source from CRMS over a decade network monitoring station. Therefore, the magnitude of regional-scale data size and density offers unprecedented opportunities for studying present coastal wetland ground elevation dynamics along with the spatial patterns and delicate interplay between the wetland ecosystem process and RSLR. Thus, a large-scale quantitative assessment of how environmental variables impact ground elevation in coastal wetlands is needed.

2.1.3 Objective

Few efforts have been made to evaluate the nonlinear relationship between environmental drivers and ground elevation. This study aims to provide an approach for quantifying ground elevation in coastal wetlands under different environmental drivers. This chapter aims to develop a ground elevation dynamic model by considering ground elevation data from 2008 to 2018 as functions of environmental variables derived from the CRMS monitoring station network in Louisiana. Additionally, this study evaluates three machine learning algorithms, including Random Forest (RF), Support Vector Machine (SVM), and Artificial Neural Network (ANN), compared to the MLR model in order to analyze statistical relationships between observed ground elevation and environmental variables, including hydrologic variables, vegetation variables, and site-specific variables.

2.2 Study area and data

2.2.1 Study area

The study area covers the entire coast of Louisiana, including the Mississippi Deltaic Plain to the east and Chenier Plain to the west, and encompasses nine hydrologic basins separated largely by current or abandoned distributary channels (Reed, 1995). The Mississippi Deltaic Plain was formed by the active deltaic lobe, which is divided into six hydrologic basins, including Pontchartrain, Breton Sound, Mississippi Delta, Barataria, Terrebonne, and the Atchafalaya basin from east to west. On the other hand, Chenier Plain was formed by periods of westward down drift of sediments deposited on a series of beach ridges and mudflats and is comprised of the Teche/Vermilion, Mermentau, and Calcasieu/Sabine basins. There was an increase in wetland area in the active deltaic lobes, including fresh, intermediate, brackish, saline, and swamp marsh types (Steyer et al., 2003). 390 CRMS monitoring station sites were initiated from fixed annual sampling design and cover the entire Louisiana coast (Figure 1.1).

2.2.2 Data

These study data provided through Louisiana's CRMS comprise an open-source regionally contiguous dataset. At each of the 390 CRMS sites, the same suite of ecological variables is collected at intervals specific to each data type, including vegetation species composition and percent cover, hourly hydrologic information, surface elevation change, and vertical accretion. Site establishment and data collection methodology are described in Folse et al. (2018).

2.2.2.1 Ground elevation measurement

The ground elevation measured by RSET was implemented within the CRMS in 2007. The RSET instrument consists of a benchmark rod driven through the soil profile to resistance, insertion of a collar for a movable horizontal arm connection, and fiberglass pins for measuring ground elevation (Lynch et al., 2015). After installing the RSET mark, the height of the pins is measured twice a year. This method has been used to generate ground elevation data since 2007 (Folse et al., 2018). RSET pin measurements are transformed into vertical NAVD 88 datum using Equation 2.1 (Lynch et al., 2015).

$$Ground\ Elevation = A - RTC + B + C - D \qquad \text{Equation 2.1}$$

As shown in Figure 2.2, “A” is the elevation of the top of the rod measured by real-time kinematics (RTK) using NAVD 88 datum surveyed in the fall of 2014. “RTC” is the rod to the collar, which is measured every time a sample is taken. The parameter "B" is the height between the horizontal table to the collar. “C” is the observed pin height; “D” is the length of the pin. The ground elevation in 2014 was used as the base elevation and adjusted with the elevation change from pin height data to generate ground elevation from 2008 to 2018.

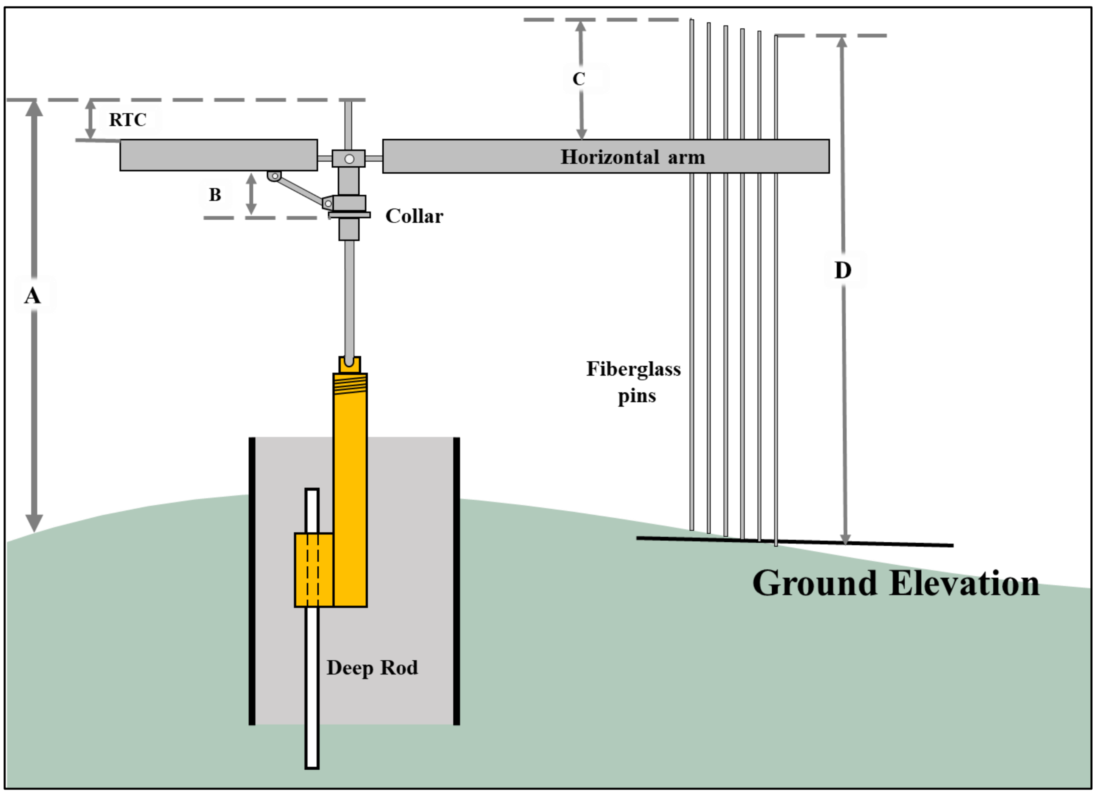

Figure 2.2 Diagram displaying steps involved in transferring RSET measurements to NAVD 88 datum. Adapted from Lynch et al., 2015.

2.2.2.2 Environmental Variables Data

The various combinations of environmental drivers and processes controlling coastal wetland ground elevation. In order for quantifying analysis of environmental drivers' impact on ground elevation, this study incorporates environmental variables to indicate and quantify the impact from the significant drivers on ground elevation. Environmental drivers were classified into environmental variables, including hydrologic variables, vegetation variables, and site-specific variables, such as distance to the main water source, for modeling ground elevation. Different environmental variables result in differences in sediment supply, primary production, decomposition, and auto-compaction, causing variations in sediment elevation among coastal wetlands (Cahoon et al., 2006). Both hydrologic variable and vegetation variable data were derived from CRMS station monitoring data collected from 2008 to 2018 (Folse et al., 2018). Site-specific variables were generated by measuring the distance between CRMS stations and the nearest water source in ArcGIS 10.7 using the State Water Bottoms dataset from the State of Louisiana Division of Administration (https://www.doa.la.gov/Pages/osl/GIS-Data.aspx).

Surface water temperature, salinity, and water level are considered hydrological variables in this study. Hydrographic data were measured concurrently with ground elevation since 2008. Surface water temperature, salinity, and water level are the indicators which contribute to above-ground biomass, productivity, and organic matter accumulation that impact ground elevation (Morris, 2006; Morris et al., 2002). Water temperatures were measured in degrees Celsius and salinity was measured in parts per thousand as calculated from specific conductance. Finally, the water levels were measured in meters relative to the instrument sensor and converted to the NAVD 88.

Vegetation variables include canopy cover percentage and average height of dominant vegetation in a sample size of 4 m^2 (Folse et al., 2018). High vegetation variables could positively impact sediment deposition and consolidation to contribute to vertical accretion (Cahoon, 2006; McKee et al., 2007; Morris et al., 2002; Nyman et al., 1993; Perry et al., 2009; Webster and Lemckert, 2002). Generally, vegetation variables indicate organic matter production, which would facilitate ground elevation in coastal wetlands (Perry and Mendelssohn, 2009). Finally, the site-specific variable contains the distance from the main water source for each CRMS monitoring station, generated in ArcGIS 10.7 using point to polygon. The distance to the main water source influences the suspended sediment loads for deposition.

2.3 Methodology

The ground elevation model is based on the statistical relationship between observed ground elevation and environmental variables using machine learning regression algorithms. The ground elevation measurements of coastal wetlands observed biannually from 2008 to 2018 are the response variable, and the hydrological variables, vegetation variables, and site-specific variable are potential explanatory variables. The entire dataset was split into training data and validation data. Data splitting involves partitioning the data into a training dataset used to generate the model and a validation dataset held aside and used to evaluate the performance of the model on unseen data. A calibration dataset which is 80% of the dataset generated for training for optimizing and training the models, and 20 % of data is the validation dataset to evaluate model performance. The training dataset was tested with MLR and three machine learning regression algorithms, including RF, SVM, and ANN, using the caret package in the open-source statistical software tool RStudio (Kuhn et al., 2016). The performance of each model was evaluated based on quantitative measures such as the Mean Absolute Error (MAE), Root Mean Squared Error (RMSE), and correlation coefficient (r). The primary process includes a split-out validation dataset, evaluates and compares different algorithms to choose the best performance model, algorithm tuning to improve accuracy, and predictions on the validation dataset. A framework was designed for the ground elevation modeling as shown in Figure 2.3.

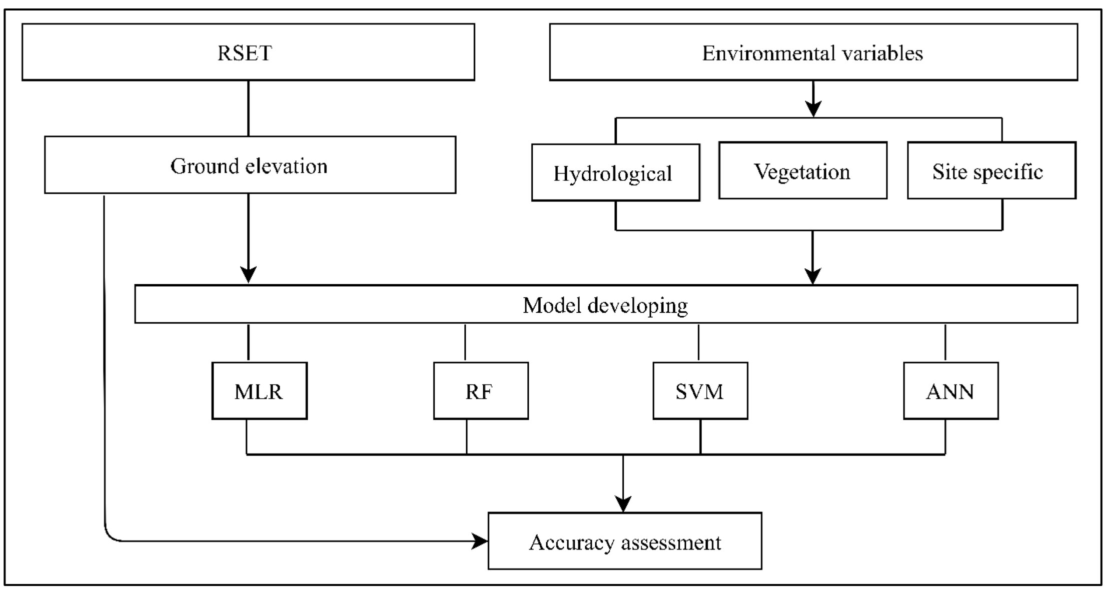

Figure 2.3 Framework for evaluating machine learning algorithms (RF, SVM, and ANN) compared to MLR for analyzing the statistical relationship between ground elevation and environmental variables.

2.3.1 *Generating ground elevation model and evaluation algorithms*

In the training dataset, the repeated k-fold cross-validation method was applied to estimate the accuracy of different machine learning regression algorithms. This study applied 10-fold cross-validation with three repeats to estimate the accuracy of different machine learning algorithms, which is a common standard configuration for comparing models. Each subset is held out while the model is trained on all other subsets, and this process is repeated three times until accuracy is determined for each instance in the dataset. The final model accuracy is taken as the mean from the number of repetitions.

In order to generate the most accurate ground elevation model, this study evaluated diverse algorithms on the training dataset. Evaluation metrics provided by the caret package in the open-source statistical software tool RStudio were used for evaluating both the linear and nonlinear algorithms on regression training data. The linear algorithms make large assumptions about the form of the function with a higher bias but are faster in training the data. On the other hand, machine learning algorithms make fewer assumptions about the underlying function and have a higher variance and higher flexibility with higher accuracy compared to linear regression. Three machine learning algorithms were chosen for their diversity of representation and learning style, which are SVM, RF, and ANN. Each model used the same training scheme and contained the evaluation metrics for each fold and each repeat for each evaluated algorithm. MAE, RMSE, and r were used to evaluate the fitness of predictions to the observation.

2.3.2 *Model validation*

The accuracy of the model prediction on data unseen during training was used as an estimate for the accuracy of the finalized model. The 20% validation data were held aside and used for evaluating the capability of the final model to predict ground elevation. The association between the model-predicted ground elevation (P) and observed ground elevation measured by RSET (O) was evaluated by several correlation, difference, and summary measures. The correlation of degree of association between P and O was expressed as Pearson's correlation coefficient (r), equal to 0 for no-fit model and 1 for the perfect fit model. Additionally, MAE and RMSE were evaluated as the average error of prediction and observation.

$$r = \frac{\sum_{i=1}^{n}(P_i - \overline{P_i})(O_i - \overline{O_i})}{\sqrt{\sum_{i=1}^{n}((P_i - \overline{P_i})^2}\sqrt{\sum_{i=1}^{n}((O_i - \overline{O_i})^2}} \qquad \text{Equation 2.2}$$

$$MAE = \frac{\sum_{i=1}^{n}|P_i - O_i|}{n} \qquad \text{Equation 2.3}$$

$$RMSE = \sqrt{\frac{\sum_{i=1}^{n}(P_i - O_i)^2}{n}} \qquad \text{Equation 2.4}$$

2.4 Results

2.4.1 Model performance

The training dataset has 730 samples with six predictors, including CRMS monitoring station distance to the main water source, average dominant plant height, percentage of plant cover, water elevation, water salinity, and water temperature, that were subjected to 10-fold cross-validation repeated three times. This study compared the estimated accuracy of different machine learning algorithms, including RF, SVM, and ANN, compared to MLR. In order to apply the optimal machine learning method to predict ground elevation, it was necessary to tune the specific parameters for each algorithm in RStudio. The caret package facilitated tuning, to reduce the likelihood of overfitting which compare the RMSE, MAE, and r for choosing the tuning parameters.

RF has two parameters for optimization, the number of trees set as 2501 and the number of variables for each node set as 10. The main parameter to tune for SVM is the cost set as 2 and sigma as 0.505, which determine the complexity of the decision boundary. Finally, for ANN, the optimal size parameter was 3 with a decay value of 0.2. The performances of these models in predicting ground elevation using environmental variables are shown in Table 2.1. RF regression achieved the best result with RMSE = 10.8 cm, MAE = 8.4 cm, and r = 0.74. SVM model produced the next highest accuracy with RMSE = 13.8 cm, MAE = 11.4 cm, and r = 0.47. The MLR and ANN produced the lowest accuracy with r of 0.43 and 0.44, respectively. Based on these results, the RF algorithms were promising for ground elevation dynamic modeling with the highest r and lowest RMSE and MAE compared to other modeling algorithms. Therefore, the tuned RF model was applied for accuracy assessment on the validation dataset.

Table 2.1 Model performance for ground elevation explained by environmental variables based on 10-fold cross-validation. The best result is in bold type.

Models	RMSE (cm)	MAE (cm)	r
MLR	14.3	11.46	0.43
RF	**10.8**	**8.4**	**0.74**
SVM	13.8	11.4	0.47
ANN	14.0	11.1	0.44

2.4.2 Feature importance for ground elevation building

The overall feature importance explains the impact of environmental variables on the ground elevation dynamic model. The RF algorithm every node is a condition of how to split value in a single feature for similar dependent variable is able to end up in the same set after the split. In regression, this condition is based on the feature variance. Using "feature importance" analysis in RStudio provides how much each environmental variable contributes to decreasing the weighted impurity. Figure 2.4 shows the top four most important features, which are the distance from site to main water source, salinity, dominant vegetation height, and water elevation. The distance from site to main water source includes the closest river, lake, or ocean which directly impacts sediment deposition. The closer the station to the water source, the higher chance for sediment deposit at the area. In addition, water salinity and elevation contribute to above-ground biomass and plant productivity. Ground elevation is positively correlated with above-ground biomass because it traps sediments suspended in water columns. The dominant vegetation height represents the health of the coastal wetlands and the ability to reduce the velocity of tidal flow and waves for sediment deposition, which promotes ground elevation.

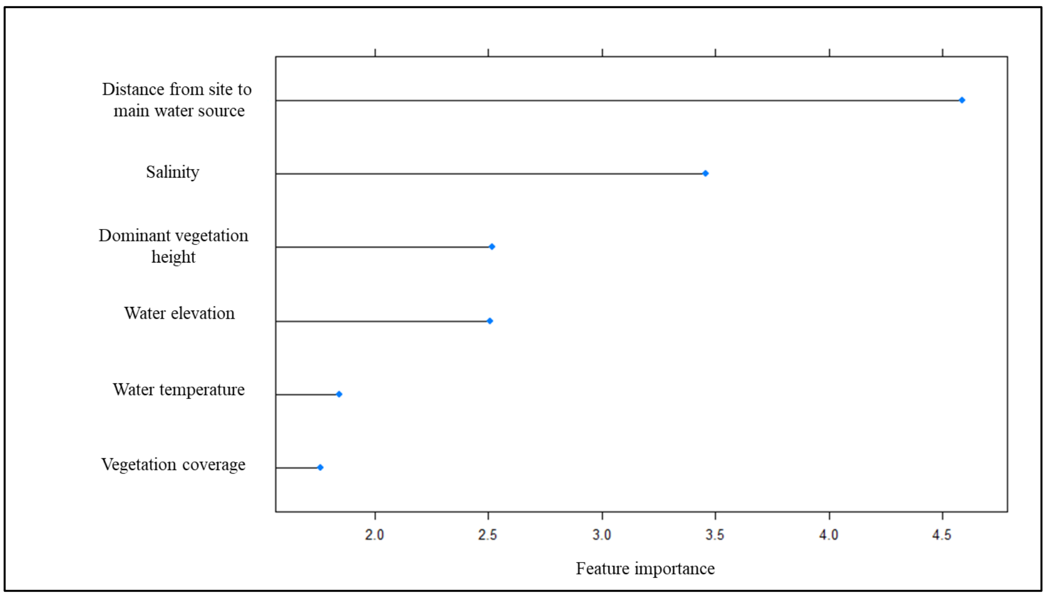

Figure 2.4 The overall feature importance of the environmental variables explaining the ground elevation dynamic model.

2.5 Discussion

2.5.1 Machine learning regression for ground elevation modeling

The results of this study show that the RF algorithm was better than a parametric method in ground elevation dynamic modeling. The RF, SVM, and ANN machine learning regression algorithms were compared to MLR. The modeling shows a diversity of performance primarily caused by differences of the algorithms. RF seeks optimal decision trees to group data, while SVM looks for an optimal hyperplane to minimize training errors and ANN models data as the structure of neurons and synapses of the human brain. The RF model achieved the best result with r = 0.74, RMSE = 10.8 cm, and MAE = 8.4 cm. SVM followed with r = 0.47. However, both ANN and MLR showed the lowest r. RF provides a promising method for explaining the non-linear statistical relationship between environmental variables and ground elevation dynamics.

Figure 2.4 shows the overall feature importance of the environmental variables for building the ground elevation dynamic model. The top four most impactful features on ground elevation were distance from site to main water source, salinity, dominant vegetation height, and water elevation. The distance from monitoring station to the closest water source may have been most important because it impacts the suspended sediment loads available for inorganic matter deposit (Roger et al., 2012). Field studies have demonstrated that the closer the site to the sediment source, in this case the closest water source, the higher chance for sediment deposit and ground elevation building (Kirwan and Murray, 2007; Chmura and Hung, 2004;) In addition, both water salinity and water elevation impact plant survival and plant productivity. Higher water elevation and higher salinity will affect vegetation colonization and if the level continually exceeds the threshold of submergence duration for vegetation survival, it will gradually cause plant mortality as well as convert emergent vegetation into intertidal mudflats or open water (Eleutherius et al., 2006). Finally, dominant vegetation height is an indicator of overall vegetation health in the coastal wetlands, which has a positive impact on ground elevation. Plants in coastal wetlands act to slow tidal flows and trap and bind deposited inorganic matter from close water sources and organic matter to promote vertical accretion (Roger et al., 2015).

Although Figure 2.1 illustrated how many environmental drivers influence coastal wetland ground elevation development, this study did not incorporate SLR, storm, and human environmental drivers due to lack of data. A challenge still remains to quantify the various effects of these environmental drivers on ground elevation in this complex coastal wetland ecosystem. In particular, storms have long been recognized as events that can cause significant geomorphological changes to coastal wetlands (Roger et al., 2015). During storms, river run off generated by severe precipitation can introduce freshwater that reduces salinity and nutrients in coastal wetlands (Day et al., 2007). Hurricanes Katrina and Rita were the fourth and fifth most powerful storms to strike the Mississippi deltaic plain and deposited 5 to 10 cm of sediment (Turner et al., 2006). On the other hand, storms can cause soil volume compaction, erosion, and sediment redistribution, which negatively impact ground elevation (Cahoon, 2006). Although there is considerable lag in the availability of data to undertake highly sophisticated modeling to assess these environmental drivers, future studies may be able to address these limitations once data are available.

2.5.2 Implication for coastal wetland planning

This study's objective was to apply machine learning algorithms to quantify the non-linear relationships between environmental variables and ground elevation, as the study has shown that the most important environmental variable is the distance from the monitoring station to the closest water source. The closer monitoring stations to the water source, including river, lake, and coastal, the more inorganic sediments could deposit and build up ground elevation. However, Louisiana has been extensively modified by humanmade constructions that alter the timing and amount of river flow to the coastal wetlands (Day et al., 2007). Since 1990, the rate of lost coastal wetlands in coastal Louisiana is as high as 100 km^2 per year (Day et al., 2007). The main cause of coastal wetlands loss was the isolation of the river from Mississippi Deltaic Plain and river almost entirely leveed to preventing overbank flooding (Day et al., 2007). Moreover, the construction of flood control significantly reduced the sediment supply from both suspended and bedload transport to the coastal wetlands (Blum and Roberts, 2009). Coastal restoration will be more effective if it takes consideration of freshwater supply and sediment into the coastal wetlands. The coastal wetland restoration should work cooperatively with better management and restore the Upper Mississippi Rivers, the reconnection of wetlands, and flood plains (Hall et al., 2003). Furthermore, with accelerated SLR, precipitation patterns, and changes in frequency and intensity of the hurricane, the ground elevation dynamics in coastal wetlands are complex and require further analysis.

2.6 Conclusion

The primary purpose of this study was to evaluate the statistical relationships between environmental drivers and ground elevation in coastal wetlands in Louisiana. The comprehensive monitoring data from 2008 to 2018 from CRMS provided more than ten years of empirical ground elevation measurements that incorporated all the mechanisms that influence ground elevation. This study designed a robust approach that evaluated one linear regression, MLR, and three machine learning regression models, including RF, SVM, and ANN. Machine learning techniques are effective at generating accurate ground elevation models from environment variables. The RF model achieved the best accuracy ($r = 0.74$ and RMSE = 10.8 cm). The outcome of this research provided a comprehensive understanding of how environmental variables impact ground elevation in coastal wetlands over time. Importantly, by analyzing ten years of statistical relationships between environmental variables and ground elevation, this study provided a robust method for predicting coastal wetlands restoration status and the response of coastal wetlands to SLR in the future.

CHAPTER 3: OBJECT-BASED LIDAR DEM CORRECTION USING RSET DATASET AND MACHINE LEARNING ALGORITHMS

3.1 Introduction

3.1.1 Significance of LiDAR derived DEM in Coastal Louisiana

Coastal wetland vegetation communities include salt marshes, brackish marshes, fresh marshes, and mangroves that exist within a narrow range of ground elevation. Additionally, coastal areas are increasingly vulnerable to wetland loss due to the combination of global sea-level rise (SLR) and local subsidence in Louisiana (Rybczyk and Cahoon, 2002). The ability of tidal wetland plant communities to successfully maintain their position is tied with their ground elevation change rate compared to rising sea-level rates (Gesch, 2009; Kirwan et al., 2016). Restoration of coastal Louisiana wetlands requires high accuracy digital elevation models (DEM) to monitor ground elevation and identify local areas vulnerable to rising sea level.

Airborne Light Detection and Ranging (LiDAR) is an active remote sensing technology that uses laser penetration and has been recognized as a standard method for generating high spatial resolution DEM (Kulawardhana et al., 2014). The DEM is a collection of square pixels where the pixel value is the value of LiDAR last return. However, research has demonstrated a decreased ability for the LiDAR laser pulse to penetrate through the vegetative layer in coastal wetlands, which are dominated by relatively low, dense, and heterogenous halophytic vegetation (Hladik and Alber, 2012). Currently, the vertical error of LiDAR systems generally ranges from 0.10 to 0.20 m

(Hodgson and Bresnahan, 2004)**,** but the vertical error in LiDAR-derived DEM in high-density vegetation can be up to 0.31 m (Hladik and Alber, 2012; Montané and Torres, 2006). These uncertainties can potentially result in misuse of the LiDAR data and erroneous conclusions (Schmid et al., 2011). Uncorrected LiDAR-derived DEM cannot meet the accuracy requirements to distinguish topographic changes in coastal wetlands at the resolution for SLR inundation vulnerability analysis (Hladik and Alber, 2012).

3.1.2 Current methods for correcting DEM

Previous modeling techniques to calibrate LiDAR-derived DEM and increase the accuracy of estimating topography include: 1) minimum bin gridding method to filter and classify LiDAR last return signals in order to reduce bias based on canopy height, density, and above-ground biomass coverage (e.g., Medeiros et al., 2015; Schmid et al., 2011;Wang et al., 2009; Töyrä et al., 2003); 2) subtraction of species-specific bias based on vegetation cover maps (e.g., Hladik and Alber, 2012; Hladik et al., 2013; McClure et al., 2016); 3) using full-waveform LiDAR data with nonparametric modeling techniques. In addition to these modeling techniques, more supplemental datasets have been used to calibrate LiDAR-derived DEM, including field-based ground elevation, real-time kinematic (RTK) and differential GPS (DGPS).

Due to high-density vegetation, only 2-3% of LiDAR lasers can penetrate through the vegetation canopy to hit the ground, then return and record the true ground elevation during LiDAR sensor data collection (Wang et al., 2009). Many algorithms have been developed for the separation of ground and nonground laser hits (Streutker and Glenn, 2006; Zhang and Whitman, 2005). The minimum bin gridding method assumes that ground elevation changes are relatively gradual; the lowest LiDAR elevation in a userspecified search window is identified as ground elevation and assigns that value to an appropriate DEM grid cell (Streutker and Glenn, 2006). The key step in this filtering method is to determine the size of the filter search window to remove the laser returns that have been reflected by the canopy rather than true ground and ultimately collect laser hits on the ground. The ideal size of the window is minimized to ensure a high spatial resolution, but is still large enough to contain enough LiDAR laser hits on the ground (Wang et al., 2009). Wang et al. (2009) used differential GPS (DGPS) as field ground reference elevation to match the ground-reflected LiDAR elevations. Each DGPS is the center point with an increasing radius from 0.5 to 6.5 m as a search window, comparing the elevation of each DGPS to the surrounding LiDAR points falling within the search window. As the radius increases, the probability of ground LiDAR returns increases, but the resolution will decrease. Thus, the optimal radius was assumed to be the smallest radius to give rise to the best attainable match between DGPS and the lowest LiDAR elevation. The overall Root Mean Square Error (RMSE) was computed for each DGPS and selected smallest LiDAR values in each radius to determine the ideal radius. The application of Wang et al. (2009) determined that a 3.5 m radius for the search window is the optimal radius for bare-earth LiDAR data filtering to improve the estimate of ground elevation in coastal wetlands.

Compared to subtracting a global elevation bias from LiDAR-derived DEM, subtraction of species-specific bias based on vegetation cover can vastly improve DEM accuracy (e.g., Hladik and Alber, 2012; Hladik et al., 2013; McClure et al., 2016). In Hladik and Alber’s 2012 study, LiDAR system with higher pulse rate frequencies and evaluated accuracy with field-based elevations RTK developed species-specific offsets for ten vegetation cover classes, which cover the entire marsh vertical range. Compared with RTK measured ground elevation, the mean vertical errors of uncorrected LiDAR-derived DEM are from 0.03 to 0.25 for different vegetation covering (Hladik and Alber, 2012). For each ground control point, LiDAR-derived elevation was derived from original LiDAR-derived DEM in grid cells as predicted elevation, and RTK measured elevation as true ground elevation. Subtracting the RTK measured ground elevation from LiDAR-derived elevation is the mean error for each ground control point. The mean error for each vegetation cover class comprised the species-specific correction factors. The mean error for each vegetation cover class comprised the species-specific correction factors. These correction factors were then applied in the subsequent DEM modification and have reduced the overall mean error from 0.10 ± 0.12 m to -0.01 ± 0.09 m and RMSE from 0.16 m to 0.1 m (Hladik and Alber, 2012).

In addition to using RTK field data, more studies incorporate hyperspectral imagery in the wetland environment (Schmidt and Skidmore, 2003; Hladik et al., 2013). Analyzing the electromagnetic spectrum and plant spectral signatures classify the wetland vegetation species as a basis for applying the species-specific correction factors to improve LiDAR-derived DEM (Schmidt and Skidmore, 2003). For example, Hladik et al. (2013) used hyperspectral data for vegetation cover classification with LiDAR-derived DEM, and the modified DEM accuracy has been improved with RMSE decreasing from 0.15 to 0.1 m. The result suggests that combine hyperspectral image in correcting LiDAR-derived DEM could effectively improve the vertical accuracy.

In the study Rogers et al., 2018, the full-waveform LiDAR applied on the high-density vegetation. Unlike traditional LiDAR, full-waveform LiDAR equipment records a time series of backscattered energy with a digitizer and high-capacity storage to generate denser point clouds (Rogers et al., 2018). By applying full-waveform LiDAR feature-based metrics (waveform width and amplitude), vegetation characteristics (slope and rugosity), and distance from the shoreline as inputs to examine nonparametric modeling algorithms. The modeling methods included Stochastic Gradient Boosting of Trees (TreeNet), Multivariate Adaptive Regression Splines (MARS), generalized path seeker model, Random Forest (RF), Classification and Regression Tree (CART), and one parametric model which was stepwise least squares regression. The corrections were performed on a point-by-point basis to reduce systematic errors due to vegetation cover and effectively dropped RMSE from 0.33 to 0.07 m (Rogers et al., 2018). Additionally, applying nonparametric modeling on a location-specific, point-by-point basis successfully eliminated a majority of the vegetation-induced bias in LiDAR-derived DEM processes.

The above studies are important contributions to calibrating LiDAR-derived DEM and increasing the accuracy of estimating topography in coastal wetlands. Current modeling techniques range from minimum bin gridding, subtracting species-specific correction factors, using full-waveform LiDAR data with nonparametric modeling, and using vegetation index from multispectral imagery (Buffington et al., 2016; Göpfert et al. 2006; Hladik and Alber,2012; Hladik et al., 2013; Medeiros et al.,2015; Montané and Torres, 2006; Populus et al., 2001; Rogers et al., 2016; Rosso et al., 2006; Schmid et al., 2011; Wang et al., 2009) (Table 3.1). However, some knowledge gaps still remain. Previous attempts to apply the minimum bin gridding method to extract lowest LiDAR elevation in an optimal search window were hindered by the dearth of true ground returns from low ground vegetation and potential inaccuracies introduced by uncertainties during separating LiDAR ground and vegetation returns (Rogers et al., 2018). On the other hand, subtraction of species-specific correction factors based on vegetation cover would apply the appropriate amount of correction to improve DEM accuracy (e.g., Hladik and Alber, 2012; Hladik et al., 2013; McClure et al., 2016). Unfortunately, the requirement of species distribution data from hyperspectral imagery or fieldwork vegetation surveys is typically unavailable or expensive to achieve (Rogers et al., 2018). Additionally, LiDAR uncertainty in wetlands environments is influenced by vegetation height, stem density, and biomass; a constant species correction factor could not meet the continuous distribution of elevation uncertainty (Rogers et al., 2016).

Recently, using advanced full-waveform LiDAR features and vegetation characteristics as inputs to examine nonparametric modeling algorithms and correcting LiDAR data point-by-point effectively reduced the systematic errors due to vegetation cover. However, a broad collection of full-waveform LiDAR is still relatively rare and requires extensive processing skills (Buffington et al., 2016). This method also often fails to produce the desired level of elevation correction for SLR required accuracy (Rogers et al., 2018). More research is needed to improve LiDAR-derived DEM. Despite these needs, it is clear that data fusion with hyperspectral or multispectral imagery and field ground elevation reference through nonparametric modeling algorithms can greatly improve the accuracy of LiDAR-derived DEM in coastal wetlands.

Table 3.1 Prior attempts in developing correction techniques for LiDAR-derived DEM.

Method	Description	Limitation	Reference
Minimum bin gridding methods	Select the lowest LiDAR elevation in an optimal search window	Hindered by the dearth of true ground returns from low, sense vegetations	e.g., Medeiros et al., 2015; Schmid et al. 2011; Wang et al., 2009
Subtraction of species-specific bias based on vegetation cover maps	Apply the correction based on specific vegetation species	Data unavailable & constant species correction factor could not meet the continuous distribution of elevation uncertainty	e.g., Hladik and Alber, 2012; Hladik et al., 2013; McClure et al., 2016
Full-waveform LiDAR with nonparametric algorithms	Full-waveform LiDAR features and vegetation characteristics as inputs to exam nonparametric modeling algorithms, and correct LiDAR data point-by-point	Broad collection of full-waveform LiDAR is still relatively rare	e.g., Rogers et al., 2018

3.1.3 Significance

Traditionally, improving LiDAR-derived elevation models commonly used RTK field technology to enhance the integrity of LiDAR products and increase the accuracy of DEM in wetland environments (e.g., Hladik and Alber, 2012; McClure et al., 2016; Montané and Torres, 2006). RTK is a field-based ground elevation method capable of delivering vertical accuracy of approximately 0.02 to 0.12 m, and combining RTK and LiDAR data reduced the DEM mean error from 0.16 to 0.04 m (e.g., McClure et al., 2016). However, the RTK method is limited by small local spatial distribution and expensive labor cost, which hinders the comparability of RTK corrected LiDAR data across a regional space (McClure et al., 2016). Additionally, annual rates of SLR and wetland ground elevation change operate on a millimeter scale; using RTK corrected LiDAR data will not meet the accuracy requirement for SLR vulnerability assessment. On the other hand, ground elevation data measured by the open-source Rod Surface Elevation Table - Mark Horizon (RSET-MH) method is collected along the entire coastal wetlands of Louisiana by the Coastwide Reference Monitoring System (CRMS). RSET technology has an accuracy of 0.13 mm for measuring sediment surface elevation in wetland environments, which is around 100 times more accurate than the current RTK system (Cahoon et al., 2002b). With the broader spatial distribution of CRMS monitoring stations and high vertical accuracy, it is expected that using RSET measured ground elevation data to correct LiDAR-derived DEM will perform better than RTK in reducing the vertical error of DEM in coastal wetlands.

Researchers often correct LiDAR-derived DEM on the pixel level and extract the pixel-based independent variables for generating correction factors (e.g., Hladik et al., 2013; Hladik and Alber, 2012; McClure et al., 2016). Instead of improving DEM accuracy on individual pixels, it would be more efficient and robust to analyze an object, which is a configuration of many pixels that have similar characteristics, using Object-based Image Analysis (OBIA) (Dronova, 2015). OBIA techniques are widely used in image classification to reduce misclassification in habitats with high spatial heterogeneity, like coastal wetlands (Blaschke, 2010). However, the application of improving DEM vertical accuracy at the object level is sparse. OBIA incorporates the similar spectral and spatial characteristics pixels and provides the opportunity to match the field ground elevation into a relatively homogeneous image object. It is necessary to apply the OBIA technique to improve DEM accuracy and potentially reduce the uncertainty of positional discrepancy between LiDAR measures and field ground elevation data. Finally, few efforts have been made to apply contemporary modeling techniques to correct LiDAR ground data for DEM improvement. Contemporary machine learning regression techniques, such as Random Forest (RF), Support Vector Machine (SVM), and Artificial Neural Network (ANN), have proven effective for modeling non-parametric data in a variety of applications. It would be necessary to explore nonlinear relationships between LiDAR data and field-measured ground elevation data for improving DEM vertical accuracy.

3.1.4 Objective

Coastal Louisiana restoration efforts require accurate DEM to monitor and simulate SLR impact on ground elevation. There is a potential to apply ground elevation measured by RSET method and LiDAR data in an object-based area to reduce errors in LiDAR-derived DEM. In this study, the CRMS monitoring station with RSET measured ground elevation (127 stations) was spatially matched to each image object. It is expected that matching image objects with the CRMS monitoring station with RSET measured ground elevation is more representative of a vegetation community than matching individual grid. This study aims to develop a machine learning approach to correct LiDAR ground point data object-based for DEM products in the Chenier Plain of coastal Louisiana using RSET field survey data. Additionally, this project aimed to evaluate the increased capability of a data fusion approach using LiDAR data, aerial photography, field ground elevation data, and machine learning algorithms to increase DEM's vertical accuracy in Coastal Louisiana.

3.2 Study area and data

This study, located along the Chenier Plain of southwestern coastal Louisiana, covered approximately 2942 square miles and included the Holocene Strand plain composed of wooded beach ridges and intervening mudflat grassy wetlands (Owen, 2008). The Chenier Plain contains fresh marsh, intermediate marsh, brackish marsh, and salt marsh. The Calcasieu/Sabine, Mermentau, and Teche/Vermilion basins formed the Chenier Plain. The Chenier Plain began forming about 3,500 years ago when the Mississippi River established a westerly course, bringing large quantities of riverine sediments and depositions that resulted in the growth of the shoreline. Figure 3.1 shows LiDAR, National Agriculture Imagery Program (NAIP) 4-band Imagery, and CRMS monitoring stations distributed across the Chenier Plain. The model application area is around two square miles and located at the Teche/Vermilion basin with the majority of intermediate marshes.

Ground elevation measurements were carried out by the RSET method and overseen by the United States Geological Survey (USGS) and Coastal Protection and Restoration Authority (CPRA) (Folse et al., 2018). All survey data are vertically referenced to North American Vertical Datum of 1988 (NAVD 88) using Geoid 12 B. A total of 127 CRMS monitoring stations in Chenier Plain, Louisiana were used in data fusion object-based LiDAR point correction modeling. Remote sensing derived data sources used in this study include LiDAR and aerial imagery data. Topographic LiDAR data were collected by Aerial Services, Inc (ASI) and Woolpert in 2017 for assessing current elevation base conditions and providing a solid data platform for monitoring future episodic events. The National Oceanic and Atmospheric Administration (NOAA) LA Chenier Plain LiDAR 2017 B16 project provided the nominal pulse spacing of 0.7 m. The data developed were based on a horizontal projection of NAD 83, Universal Transverse Mercator (UTM) Zone 15N in meter, and vertical datum of NAVD 88. In order to meet ASPRS vertical accuracy guidelines, Woolpert established a total of 68 ground control points for calibrating the vertical LiDAR accuracy. The horizontal positional accuracy meets 0.355 meters, and non-vegetated vertical accuracy is 0.122 meters. On the other hand, the imagery data used in this dissertation were from NAIP, which is administered by USDA FSA for agricultural production monitoring. NAIP acquire and provide ortho imagery that has been collected during the agricultural growing season in the U.S. The imagery was collected using a Leica ADS-100 digital sensor and cameras, which are calibrated radiometrically and geometrically by the manufacturer and are all certified by the USGS. NAIP quarter quads are formatted to the UTM coordinate system using the North American Datum of 1983 with five-meter resolution. NAIP imagery are 32-bit pixels with 4 band color including red, green, blue, and near infrared.

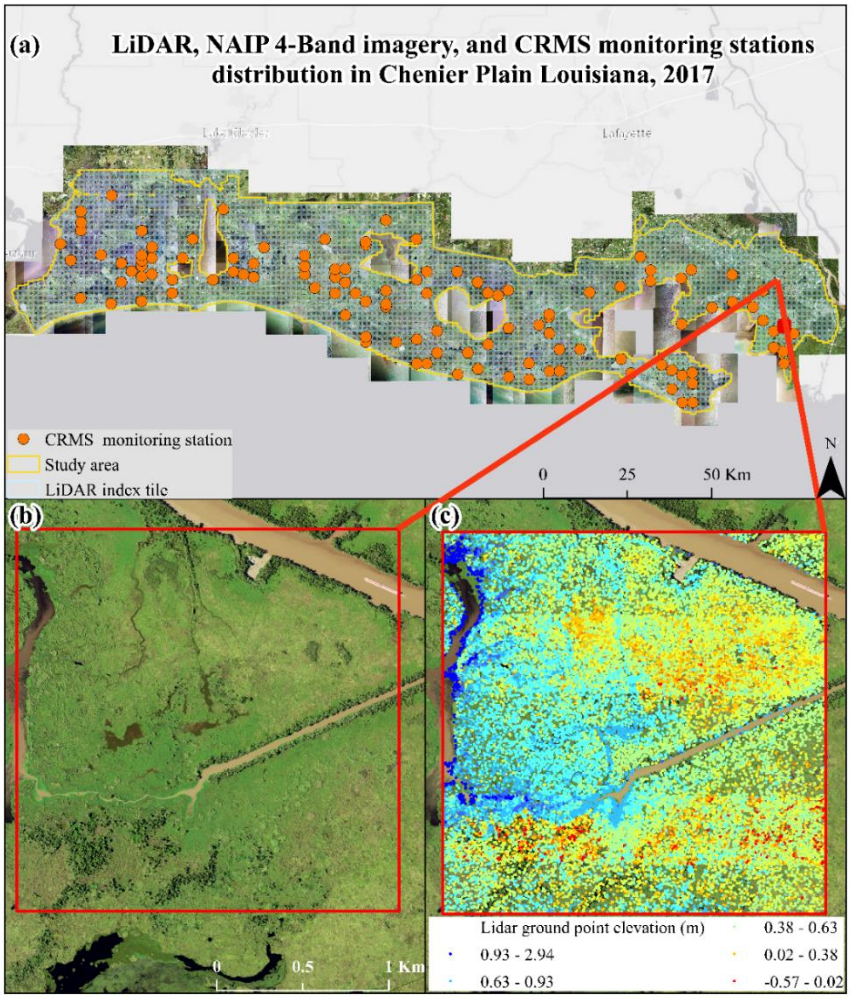

Figure 3.1 Index tiles of LiDAR and NAIP 4-band imagery with CRMS monitoring station distribution and model application area in Chenier Plain, Louisiana.

3.3 Methodology

Figure 3.2 shows the framework for object-based LiDAR derived DEM correction using ground elevation measured by RSET and machine learning in coastal Louisiana conducting object-based LiDAR correction and generating DEM. First, the ground elevation data derived from CRMS stations were spatially matched with aerial photography for image object generation by multi-resolution segmentation algorithm. The LiDAR ground point data then were spatially and temporally matched with the image objects. The matched samples, including field RSET ground elevation and LiDAR features that fall into the objects, were extracted to generate object-based data metrics and were randomly separated into training data for model calibration and testing data for model verification. RF, SVM, ANN, and Multiple Linear Regression (MLR) were applied to develop models using training data. Model performances were assessed with correlation coefficient (r), Mean Absolute Error (MAE), and RMSE. Finally, the most accurate model was applied to the study area to generate object-based DEM. Major steps in the study design included generating image objects from aerial photography data, assigning each image object its respective LiDAR statistics, matching CRMS monitoring station data with LiDAR features, LiDAR point data correction modeling, evaluating model performance, and application of model. These major steps are described in full detail in the following subsections.

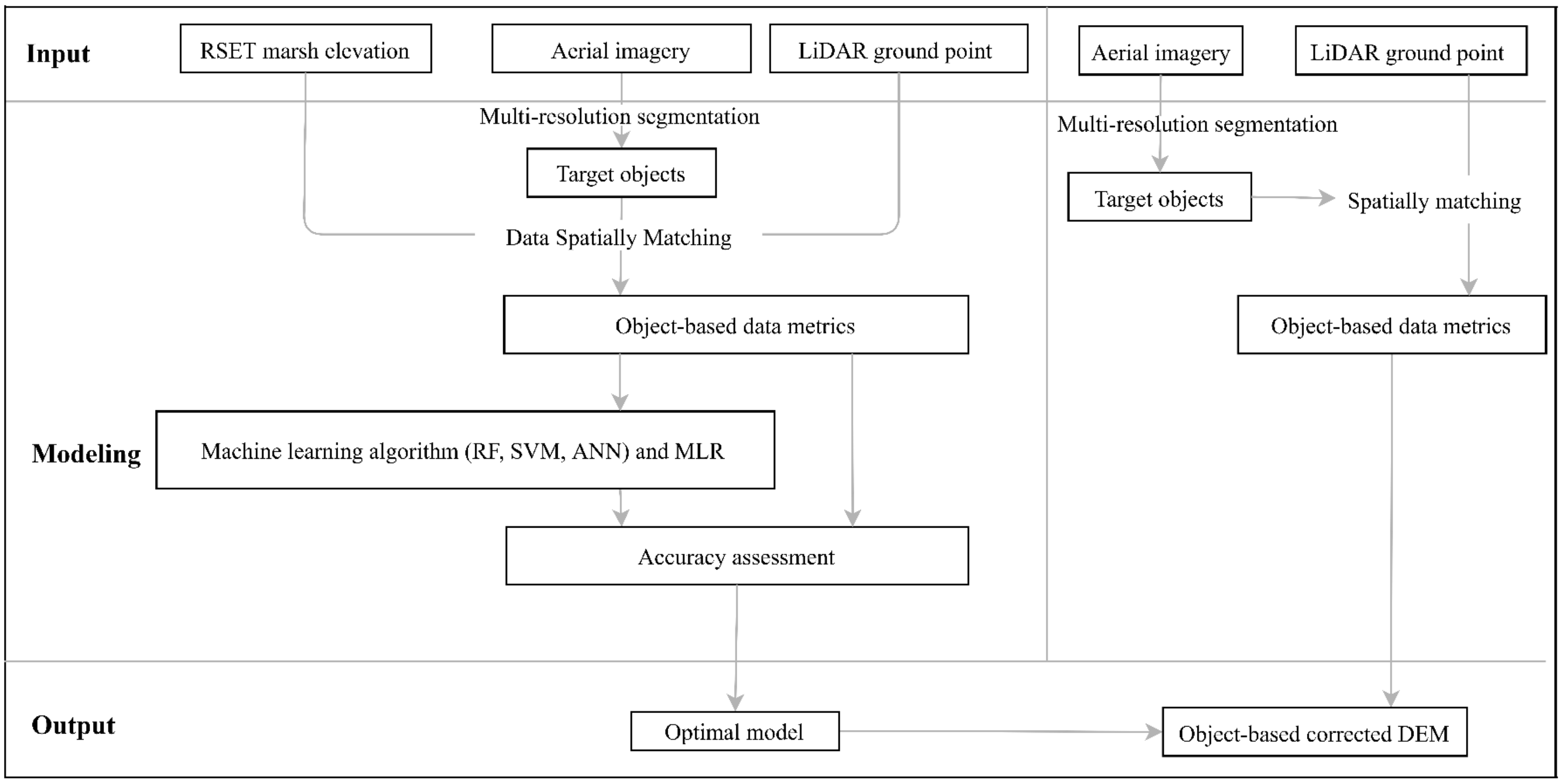

Figure 3.2 Framework for generating object-based LiDAR correction model, accuracy assessment, and application for generating object-based corrected DEM.

3.3.1 Object-based image analysis

CRMS monitoring stations were spatially matched with arial images for the generation of image objects around the station point. The object-based image analysis approach delineates segments of the homogeneous image area around the monitoring stations. The multi-resolution segmentation algorithm in eCognition Developer 9.3 (Trimber, 2017) is a region-merging technique starting with one pixel then merging neighboring pixels into objects until the heterogeneity threshold is reached (Benz et al., 2004). Throughout this pairwise clustering process, the scale, image layer weights, and composition of homogeneity criteria are the user-defined parameters determining the heterogeneity threshold (Benz et al., 2004). Among the parameters, the scale determines the maximum possible change of heterogeneity caused by fusing several objects. Thus, small scale value generates smaller homogeneous objects, and higher scale value produces larger heterogeneous objects. The optimal object is small enough for highly detailed object-based DEM generation, but large enough for adequate LiDAR ground points for statistical descriptions. Thus, for the optimal object scale, this study tested six segmentation scales, including 5, 10, 15, 20, 30, and 50. The image layer weights set all four layers (red, green, blue, and near-infrared) to 1,1,1,1 so that spectral information was weighted equally. Meanwhile, the parameter composition of the homogeneity criterion includes the shape parameter set as 0.1 and the compactness parameter set to 0.5. The final generated image objects for each monitoring station were then extracted as shapefiles for further matching with LiDAR ground points and tested as the possible independent variable for the object-based elevation models.

3.3.2 Matching LiDAR ground point data with image objects

Ground elevation data from 127 CRMS monitoring stations were spatially matched with image object polygons generated from OBIA. The "LAS Point Statistic by Area" tool in ArcGIS version 10.7.1 by Esri (www.esri.com) was used for evaluating the statistics of LiDAR ground points that fall into the image object polygon. The LiDAR ground point value (Z) statistical metrics, including the lowest Z value, the average Z value, the highest Z value, and the total of LiDAR ground points fall into the image object and the SD of Z value. Additionally, LiDAR point density was calculated as the number of LiDAR points divided by the image object area. All LiDAR statistical information was used as independent variables for ground elevation modeling and mapping. Meanwhile, the 2017 RSET ground elevations from CRMS monitoring stations were used as dependent variables.

3.3.3 Object-based LiDAR point data correction modeling

The 127 matched samples with ground elevation data and LiDAR statistic metrics in image objects were split into two datasets: 80% of the data as a training dataset for optimizing and training the models, and 20% of the data as the validation dataset to test the model performance. The ground elevations in 2017 generated from RSET measurements were the response variable. Monitoring station longitude and latitude, LiDAR point statistic metrics (including minimum, mean, maximum), LiDAR point density fall in the object, and image object area (square meters) were the potential explanatory variables. For the training dataset, three nonparametric machine learning algorithms RF, SVM, and ANN and one parametric algorithm MLR were tested using WEKA version 3.8 (Hall et al., 2009).

3.3.4 Evaluation of model performance and application

To choose the optimal models, the test data were used to produce a quantitative assessment of the final corrected LiDAR point in an image area to compare between models. The association between each corrected ground elevation (*P*) value and observed ground elevation measured by RSET (*O*) was evaluated using several correlation, difference, and summary measures. The correlation of the degree of association between P and O was expressed as Pearson's coefficient of correlation (r) and the proportion of the variance explained by P was described as the coefficient of determination (R^2). Additionally, two types of difference measures were calculated, which include the average error MAE and RMSE. Finally, the ideal modeling algorithm was applied in the application area. The statistical metrics of LiDAR ground point distribution in the OBIA object area were loaded into the WEKA supplement data for predicting ground elevation for each object. Then, each object polygon with predicted ground elevation was loaded into ArcGIS 10.6 and the "polygon to raster" feature was applied in order to generate a corrected object-based DEM.

3.4 Results

3.4.1 LiDAR point data at object level with multiple scales

In order to identify any patterns in the difference between the minimal LiDAR ground returns and observed ground elevation measured by RSET, this study applied OBIA to correct LiDAR at the object level. The object-based approach provides an opportunity for spatial features within the 4-band imagery to reduce the positional discrepancy between the image and RSET measurements, since the image object generated by OBIA represents a vegetation patch better than a single grid (Cooper et al., 2019). Applying the OBIA method to correct LiDAR derived DEM reduced local noise in the heterogeneous wetland environments, and the threshold is determined by a user-defined scale parameter (Dronova, 2015). Figure 3.3a shows an example of CRMS monitoring station 685 in different scales (5, 10, 15, 20, 30, and 50) of image objects. A smaller-scale value produces smaller homogeneous patches of image pixels, while a larger-scale parameter generates larger heterogenous patches. Figure 3.3b shows an example of CRMS monitoring station 685 LiDAR ground point distribution in each object with different scales of image objects.

To help identify any patterns in the differences between the minimal LiDAR ground returns and ground elevations measured by the RSET method, choosing the optimal scale parameter for the heterogeneous threshold is necessary. The ideal size of the object has minimized size to ensure a high spatial resolution, while still being large enough to contain enough LiDAR laser hits on the ground (Wang et al., 2009). The average number of LiDAR ground points in 127 monitoring stations with scales 5, 10, 15, 20, 30, and 50 was 40, 170, 344, 602, 1461, and 4638, respectively, as shown in Table 3.2. With a larger image object, more LiDAR ground points fall into the area while SD is reduced. The average bias between the minimal value of LiDAR ground point and ground elevation measured by RSET in scale 5 objects was the highest at 0.15 m, and bias in scale 50 objects was the lowest at -0.055. Additionally, scales 5, 10, and 50 had relatively higher RMSE and MAE compared with scales 20 and 30. Finally, the difference measures (MAE, RMSE, and bias) help to determine better object-based scale. Scale 30 datasets are preferred and have the relative lowest difference compared with the ground elevation measured by RSET. Thus, the scale 30 image object was used for evaluating the machine learning algorithm in the object-based LiDAR correction model and final application for DEM generation.

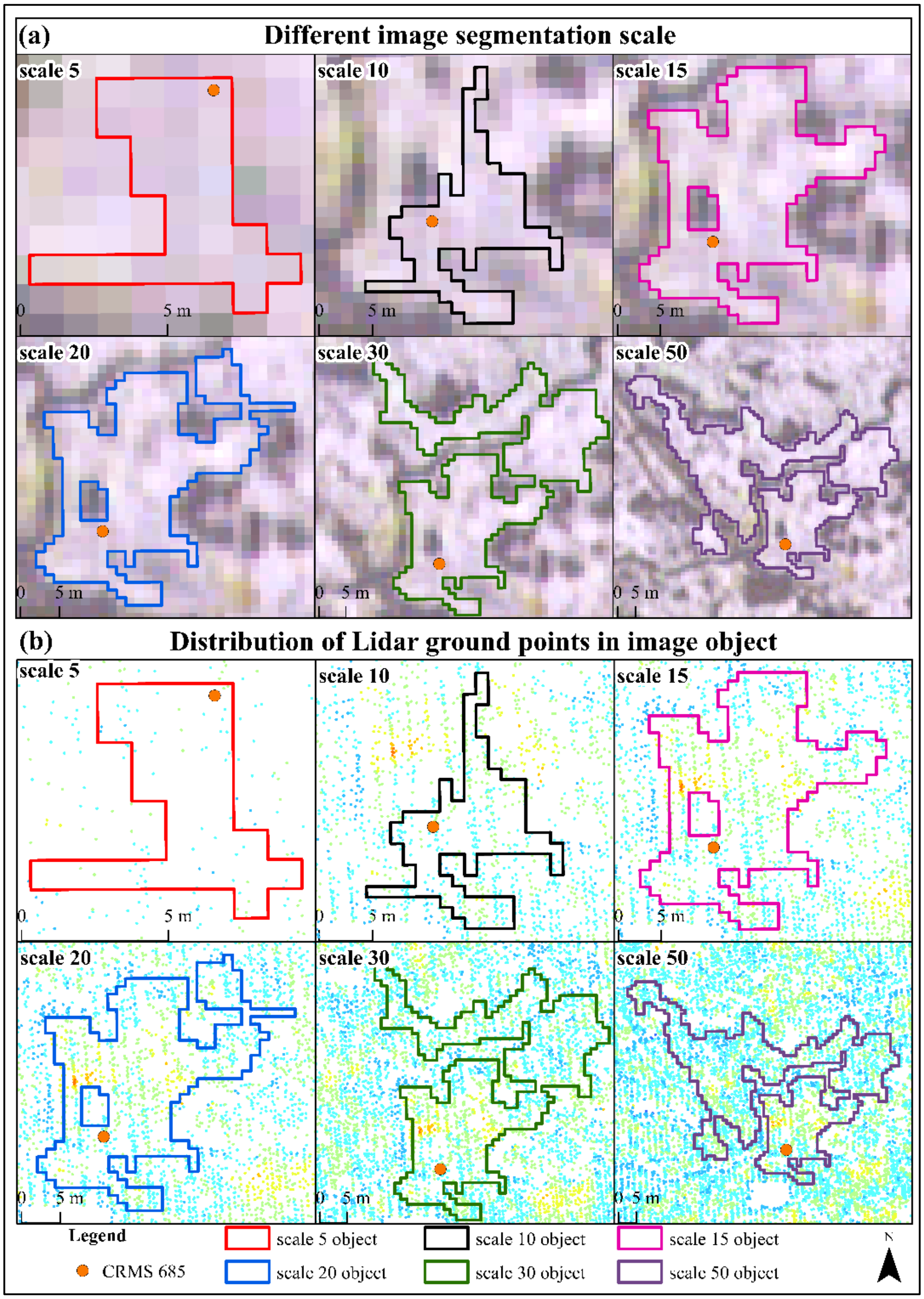

Figure 3.3 Example of CRMS monitoring station 685 in image objects with different image segmentation scales, (a); LiDAR ground point distribution in image objects with different image segmentation scale (b).

Table 3.2 Summary of ground LiDAR points and observed ground elevation measured by RSET in target objects. The table lists the average number of LiDAR ground points in each object with different segmentation scales (5, 15, 20, 30, and 50). n = average number of LiDAR points that fall into the image object, min = minimum, max = maximum, SD = standard deviation, bias = difference between the minimal LiDAR ground elevation and observed ground elevation measured by RSET, RMSE = the root mean square error between minimum LiDAR ground elevation and observed ground elevation by RSET, MAE = mean absolute error between minimal LiDAR ground elevation and observed ground elevation measured by RSET. The units are in meters except for n.

Ground elevation by RSET				LiDAR elevation in image object						Difference of LiDAR minimal elevation with ground elevation		
Total Point	min	max	mean		n	min	max	mean	SD	Bias	RMSE	MAE
127	-0.12	0.58	0.2	Scale 5	40	-0.05	0.88	0.36	0.15	0.15	0.21	0.17
				Scale 10	170	-0.24	0.65	0.29	0.15	0.09	0.19	0.15
				Scale 15	344	-0.28	0.65	0.27	0.16	0.06	0.18	0.14
				Scale 20	602	-0.28	0.65	0.24	0.17	0.03	0.19	0.14
				Scale 30	**1461**	**-0.29**	**0.65**	**0.2**	**0.17**	**-0.01**	**0.19**	**0.13**
				Scale 50	4386	-0.39	0.65	0.15	0.18	-0.06	0.22	0.15

3.4.2 Model performance for object-based DEM correction

All of the machine learning algorithms, including RF, SVM, and ANN, and MLR were implemented and tuned in WEKA, a machine learning modeling software package (Hall et al., 2009). The machine learning algorithm model predictions and ground elevation measured by RSET (observations) in scale 30 image objects are displayed in Table 3.3. RF achieved the best result with r = 0.83, which was followed by SVM with r = 0.74. The MLR and ANN produced the worst results with 0.57 and 0.45, respectively. Based on the experimental results in Table 3.3, the object-based RF machine learning algorithm was promising for ground elevation modeling with the lowest RMSE = 0.08 m and lowest MAE = 0.07 m. To further evaluate the three machine learning algorithms and MLR, the scatter plots of the ground elevation measured by RSET and RF, SVM, ANN, and MLR estimations are displayed in Figure 3.4. RF achieved the highest $R^2 = 0.69$ for the ground elevation estimation. Thus, for correcting LiDAR ground points for generating DEM, the RF algorithm was selected because it shows a significantly better prediction than other model methods. From the model results and statistical analysis, it was found that predictions from RF were ideal for correcting LiDAR ground points and DEM generated in the application area.

Table 3.3 Model performance for object-based LiDAR correction. The best result is in bold.

Models	MAE (m)	RMSE (m)	r	R^2
RF	**0.07**	**0.08**	**0.83**	**0.69**
SVM	0.08	0.10	0.74	0.55
ANN	0.15	0.2	0.45	0.21
MLR	0.11	0.12	0.57	0.33

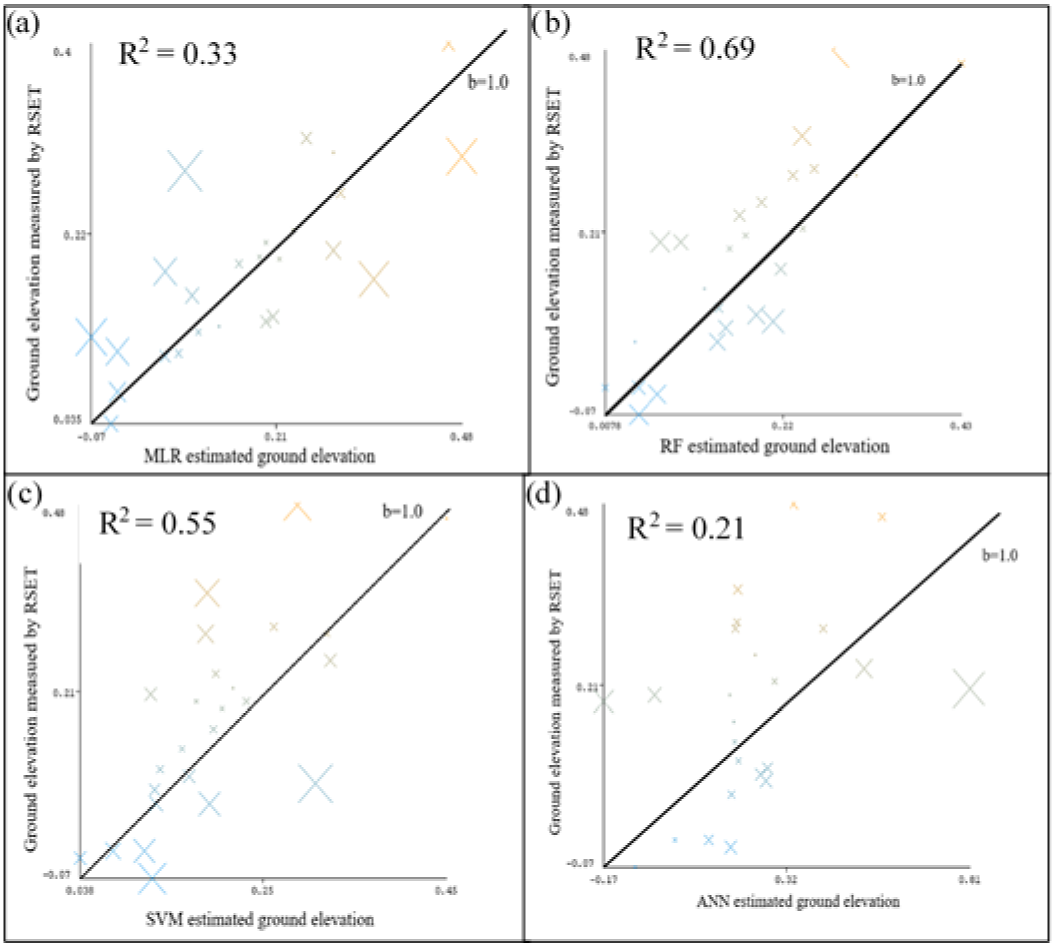

Figure 3.4 Scatterplots of ground elevation measured by RSET versus MLR (a) and the machine learning algorithm predictions including RF (b), SVM (c), and ANN (d). The perfect prediction line is the same prediction as the observation plotted as b=1.0.

3.4.3 Application of object-based RF correction for final DEM generation

These findings confirmed that object-based RF correction successfully increased vertical accuracy for LiDAR-derived DEM in coastal wetlands. The final DEM maps were derived from LiDAR ground point data in the modeling application area by applying a grid-based minimum binning method and applying the most accurate and precise models to the object-based RF corrected modeling. The DEM maps derived from the grid-based minimum binning interpolation method assume the minimum LiDAR point value in the cell as the ground value (Figure 3.5a). On the other hand, the object-based RF corrected DEM was generated from the LiDAR ground points dataset and aerial imagery. First, the image of the modeling application area was segmented into image objects with scale 30. The LiDAR ground points data were spatially matched with each image object and statistical information was extracted for RF correction modeling. By applying the optimal RF corrected model in WEKA, the corrected ground elevation in each object was generated for the final DEM (Figure 3.5b). In Figure 3.5, the red represents higher elevation above NAVD 88, and blue represents lower elevation below NAVD 88. Generally, the correction was successful in reducing the overestimation of terrain elevation throughout the test area and produced results with a higher accuracy DEM. As shown in Figure 3.5, the object-based RF corrected was able to reduce RMSE from 0.355 m to 0.08m while maintaining the general topographic pattern of the application area.

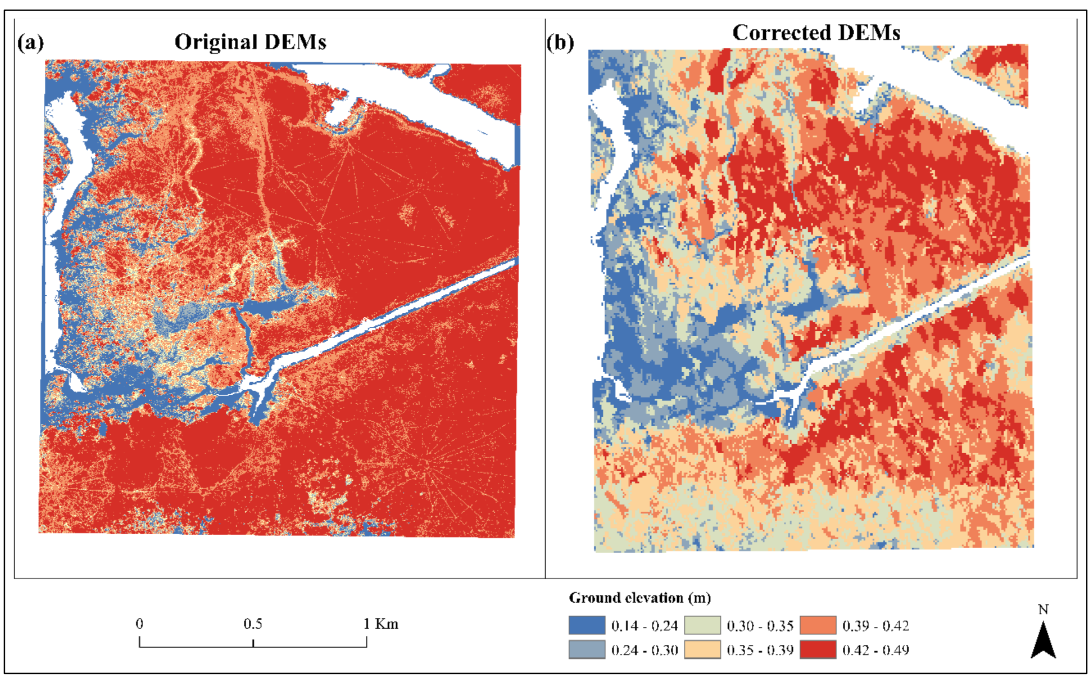

Figure 3.5 Original DEM generated by using minimum bin on a grid-based level (a); corrected DEM by applying RF correction model on an object-based level (b).

3.5 Discussion

3.5.1 Applying machine learning regression for LiDAR correcting

The recent studies from Roger et al. (2018) and Copper et al. (2018) have demonstrated that nonparametric machine learning algorithms have immense potential in LiDAR-derived DEM correction. In this chapter, RF, SVM, and ANN were evaluated and compared with MLR to increase LiDAR-derived DEM vertical accuracy in the Coastal of Louisiana. The RF machine learning algorithm generated encouraging results in predicting the ground elevation area in objects using LiDAR ground point statistical metrics, with r = 0.83 with RMSE was reduced from 0.355 m to 0.08m. Although the location of the study area is not the same, these results are comparable with the study by Copper et al. (2018) and Roger et al. (2018) study where RF is the optimal model for correcting LiDAR-derived DEM with RMSE = 0.10 m and RMSE = 0.11cm, respectively. Based on this study and the study by Copper et al. (2018) and Roger et al. (2018), the RF modeling algorithm is robust for correcting LiDAR-derived DEM. This is likely due to the nature of the RF modeling algorithm in which ensembles of randomly trained decision trees tend to produce higher accuracy on previously unseen data (Criminisi et al., 2011). The decision trees are all randomly chosen and randomly different from others, which leads to decorrelation between the individual decision tree prediction results in improved generalization and robustness (Criminisi et al., 2011).

The SVM produced an acceptable degree of association between the predicted and observed ground elevation where the r = 0.74. The SVM tends to find the optimal hyperplane to separate classes based on training samples (Huang et al., 2002). The hyperplanes can be linear or apply kernel functions for addressing the inseparability problem to optimize the nonlinear correlation (Mountrakis et al., 2011). Besides choosing the kernel function, the cost is the main parameter to tune for SVM, which determining the hyperplane's complexity. On the other hand, the ANN model produced with the lowest coefficient of correlation (r = 0.45). Even though the ANN modeling algorithm is based on neuron networks and organized into layers, the relative weight connecting adjacent layers is a challenge to train the data (Maxwell et al., 2018). Generally, the nonparametric machine learning algorithms are powerful in correcting LiDAR-derived DEM. The object-based RF model achieved the best results with the r = 0.83, which is essential for applying in future DEM generation and monitor coastal restoration and SLR analysis.

3.5.2 Applying object-based modeling for correcting LiDAR-derived DEM

Past research in correcting LiDAR-derived DEM focused on pixel-based analysis. Pixels are an arbitrary unit of analysis of image classification as it may contain mixed signals from surrounding areas (Jensen, 2015). OBIA on the other hand considers the spectral and spatial characteristics of the surrounding pixels by collecting similar pixels into an image object. In this study, object-based LiDAR points corrected for predicting ground elevations provide an attractive alternative to the commonly used pixel-based LiDAR point correction. Unlike the pixel-based DEM correction, OBIA based on spectral value, shape texture, and context information, including spatial autocorrelation, has none of the salt-and-pepper phenomena and are well developed for image classification and regression (Blaschke, 2010; Maxwell et al., 2018).

Additionally, the object-based approach provides the opportunity to match the CRMS monitoring station to an image object. The OBIA represent more ecologically relevant spectral information in object and reduce the positional discrepancy. The scale parameter is recognized as one of the most significant variables for OBIA since it determines the relative size of the image object (Drăguţ et al., 2014). The ideal image object should match an image object that can well represent the plant structure and ground condition in the plot. Using a smaller value of the scale parameter will generate a more homogenous object than a higher scale value. However, it might result in the same problem as pixel-based modeling. On the other hand, using a higher scale parameter could cause fewer homogeneous objects and fail to present the ground condition. Choosing the appropriate image object scale parameter is a challenge. In this study, different image segmentation scale parameters, including 5, 10, 15, 20, 30, and 50, were tested. The optimal image object scale is that in which LiDAR ground points are closest to the ground elevation measured by RSET with the lowest MAE and RMSE. Applying LiDAR ground points that fell in the image object to modeling and predicting the ground elevation has a higher probability of generating higher accuracy DEM.

3.6 Conclusion

The primary aim of this study was to develop an object-based approach for modeling and correcting LiDAR point data for an improved DEM product in a wetland environment by combining OBIA and machine learning algorithms. Testing results suggested this approach was promising for generating high vertical accuracy of DEM compared with the minimal bias and pixel-level modeling techniques. This study draws the following conclusions: 1) Nonparametric machine learning modeling techniques are powerful for ground elevation estimation. This study evaluated three machine learning regression algorithms, including RF, SVM, and ANN, compared to MLR. The results show that the RF model achieved the best result with r = 0.83 for ground elevation estimation and was used for the application area. 2) The object-based machine learning model correcting LiDAR generated DEM has the potential to assist other researchers. With the high vertical accuracy of 0.08 m and horizontal accuracy of 0.355 m, this model provides the baseline to monitor restoration efforts under the challenge of SLR.

CHAPTER 4: RELATIVE SEA-LEVEL RISE INUNDATAION ANALYSIS USING CORRECTED LIDAR DEM AND RSET-MH DATASETS

4.1 Introduction

4.1.1 Relative sea-level rise impacts wetlands in coastal Louisiana

Coastal wetlands are facing the imminent loss of land and ecosystem services due to detrimental environmental stress from global sea-level rise (GSLR) (Kirwan et al., 2016). With thermal expansion and ice melt, sea levels are expected to accelerate significantly over the next century (Nicholls and Cazenave, 2010; Rahmstorf, 2010). Land changes and high sea-level rise (SLR) rates are exposing the lowland coastal zone to more frequent and longer lasting saltwater submerges, rapidly eroding the shoreline, and magnifying the adverse effects of storms (Kirwan and Megonigal, 2013).

Moreover, due to geographic variation in glacial isostatic adjustment and non-uniform changes in ocean thermal expansion and land subsidence, regional trends in sea-level are not equal to GSLR (Nicholls and Cazenave, 2010). GSLR presents only one component to consider when anticipating future SLR. The SLR rate prediction in the specific coastal zone is a combination of GSLR and local processes, including natural astronomical, oceanic, and atmospheric cycles, glacial isostatic adjustment, subsidence, accretion, and erosion from shorelines (Jankowski et al., 2017). This is especially true in coastal Louisiana with the highest subsidence rate, which includes shallow and deep subsidence. At least 60% of the total subsidence rate is shallow subsidence that occurs within the uppermost five to ten meters (Jankowski et al., 2017). Shallow subsidence is primarily controlled by shallow sediment compaction when new materials are either deposited or organic matter is compacted onto the less consolidated marsh ground, causing reduced thickness and ground elevation in a relatively short time (Cahoon et al., 1995). Deep subsidence happens below 20 m underground in the compressible Holocene sediments and above the Pleistocene surface where rates are comparatively stable (Jankowski et al., 2017).

Importantly, coastal Louisiana, with a low initial elevation, has lost about 5,000 km2 of land area from 1932 to 2016 (Couvillion et al., 2016), and remaining wetlands need to compete with the highest rate of relative sea-level rise (RSLR) in the world (Jankowski et al., 2017). The extent of this threat to coastal Louisiana is poorly understood due to the lack of geographically comprehensive impact assessments. Generating high horizontal and vertical accuracy Digital Elevation Models (DEM) of coastal Louisiana for RSLR inundation mapping is crucial.

4.1.2 Existing models for assessing coastal wetlands vulnerability to SLR

Numerous modeling approaches have addressed the vulnerability of coastal wetlands under SLR impacts (e.g., Fagherazzi et at., 2006; Marani et al., 2007; Mariotti and Fagherazzi, et al., 2010). The most basic landscape models assess coastal wetlands vulnerability by applying projected SLR onto a static topographic representation of the coast, like filling water in a bathtub (Moeslund et al., 2011). The land area below the water level indicates the low-lying area, which is inevitably drowning over time (Gesch, 2009). A critical shortcoming of these bathtub style models is that they do not simulate the dynamic ecogeomorphic feedbacks that allow the coastal wetlands to adapt to SLR by accelerating rates of ground elevation change. This shortcoming results in assuming that the landscape remains constant over time (Rogers et al., 2012). A more advanced model is the Sea Level Affecting Marshes Model (SLAMM), which assumes a topographic landscape that evolves at a constant rate of ground elevation change resulting from site-specific historical accretion rates. In particular, SLAMM has been widely used by the US Fish and Wildlife Service to identify SLR threats and improve land management and land acquisition decision making.

That coastal wetlands are vulnerable to the imminent loss of ecosystem services is a feared consequence of faster SLR rates. Current Airborne Light Detection and Ranging (LiDAR) derived DEM and analyses based on ground accretion may overestimate the resilience of coastal wetlands to SLR, since uncorrected LiDAR-derived DEM normally overestimate ground elevation (Want et al., 2009). Additionally, due to the high rate of subsidence in coastal Louisiana, an accurate estimate of the current rate of subsidence would be necessary to provide a context for the planning of wetland restoration and predictions of RSLR flooding. Until recent models, numerical models of wetlands SLR generally featured a static topography that does not typically incorporate the ground elevation change that allows wetlands to adapt to SLR (Rogers et al., 2012; Schile et al., 2014; Stralberg et al., 2011; Swanson et al., 2014). Meanwhile, the bathtub style model was developed without making the site-specific predictions that are necessary to inform management decisions. It is necessary to build an effective site-specific historical rate of ground elevation change to predict coastal wetlands change more accurately.

4.1.3 Objective

The main objective of this study was to provide a high vertical accuracy relative sea-level inundation map using machine learning corrected object-based DEM as the base map, a site-specific RSLR water model, and a ground elevation model. The specific objectives of this study were: 1) To apply the object-based algorithm to LiDAR-derived DEM for generating high vertical accuracy DEM in 2017. To achieve this objective, the 2017 LiDAR ground points, National Agriculture Imagery Program (NAIP) aerial imagery, and ground elevation measured by Rod Surface Elevation Table-Mark Horizon (RSET-MH) were applied to the Random Forest (RF) correcting model from Chapter 3 to generate a 2017 object-based DEM as the base map for RSLR inundation mapping. 2) To apply monitoring to a site-specific ground elevation change model and site-specific RSLR water model on the 2017 DEM map. This was achieved by analysis of unprecedented ground elevation rates measured over ten years at 127 monitoring stations around coastal Louisiana, with annual increments to 2050 applied to the 2017 DEM base map. Meanwhile, instead of the RSLR rate generated from tide gauges, this study applied site-specific total subsidence rate, including shallow subsidence and deep subsidence, combined with GSLR rate as RSLR and annual increments to 2050 were applied to the 2017 DEM base map. 3) Generate and compare the predicted 2050 RSLR inundation map by applying 2050 RSLR on predicted grid-based minimal binning corrected DEM and predicted object-based RF corrected DEM.

4.2 Study area and data

This study area is located along the Chenier Plain of southwestern coastal Louisiana, which covers approximately 2942 square miles and includes the Holocene

Strand plain composed of wooded beach ridges and intervening mudflat grassy wetlands (Owen, 2008). The Chenier Palin contains fresh marsh, intermediate marsh, brackish marsh, and salt marsh. The Chenier Plain is comprised of the Calcasieu/Sabine, Mermentau, and Teche/Vermilion basins. Figure 4.1 shows LiDAR index tiles, NAIP 4-band imagery, and Coastwide Reference Monitoring System (CRMS) stations distributed across the Chenier Plain.

This study evaluated 127 records derived from RSET-MH measurements provided through Louisiana's CRMS (Folse et al., 2018). The CRMS monitoring network is on an order of magnitude of regionally contiguous data monitoring coastal wetland change since 2007, for the study of present-day and projecting future coastal wetland dynamics along with its uncertainties, spatial patterns, and the delicate interplay between ground elevation change and RSLR. Meanwhile, LiDAR ground point data received from 2017 USGS LiDAR shows the Upper Delta Plain, LA with 4802 single 1500 m by 1500 m tiles covering approximately 3843 square miles. The LiDAR data were collected in early 2017, with no snow present and when rivers were at or below normal levels. Meanwhile, the LiDAR data were collected at an aggregate nominal pulse space of 0.7 m with the horizontal projection of NAD 83 (2011) Universal Transverse Mercator (UTM) (zone 15 N) and vertical datum of NAVD 88 (GEOID 12B) in meters. Finally, the ortho imagery data generated by the NAIP were used for image segmentation. The images collected in 2017 were formatted to the UTM coordinate system using the North American Datum of 1983 with 32-bit pixels with four band colors with red, green, blue, and near-infrared.

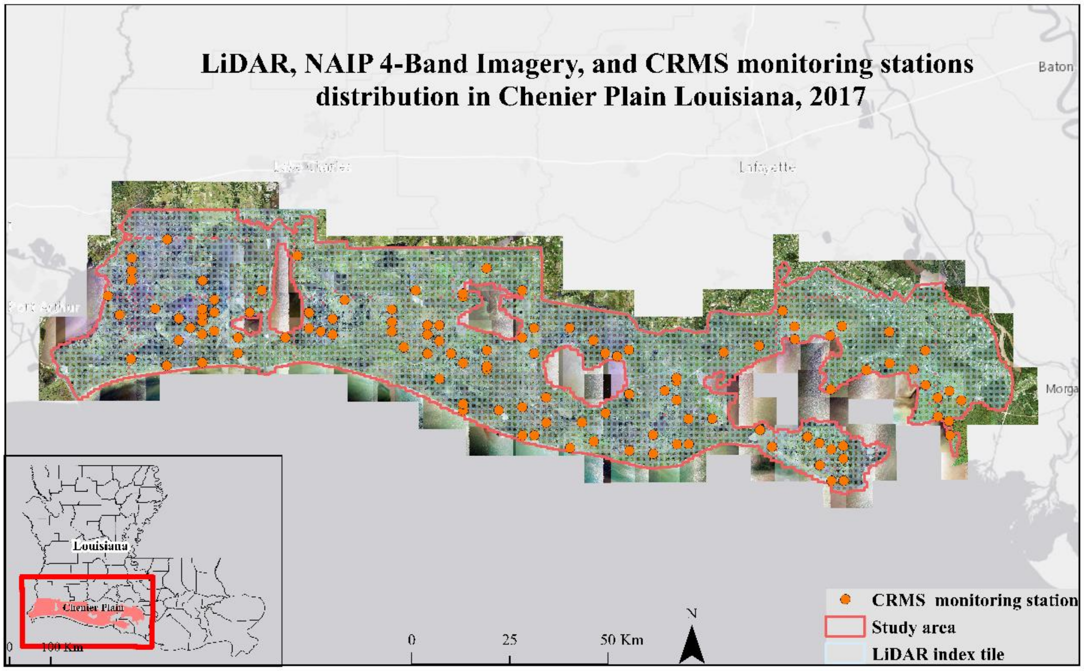

Figure 4.1 Index tiles of LiDAR and NAIP 4-band imagery with CRMS monitoring station distribution in coastal Louisiana.

4.3 Methodology

Mapping predicted relative sea-level inundation in the Chenier Plain in coastal Louisiana required three significant steps. First, grid-based and object-based machine learning corrected DEM using LiDAR ground points were generated. Second, ground elevation change rate was generated from field observed ground elevation data for each CRMS monitoring point from 2007 to 2019. Then, ground elevation change rates and relative sea-level change rates were applied on both the grid-based DEM and object-based machine learning corrected DEM. Third, the annual incremental ground elevation change rate and RSLR rate to 2050 were applied to compare differences in RSLR inundation between minimum binning grid-based DEM and object-based machine learning corrected DEM. The major steps are presented in Figure 4.2.

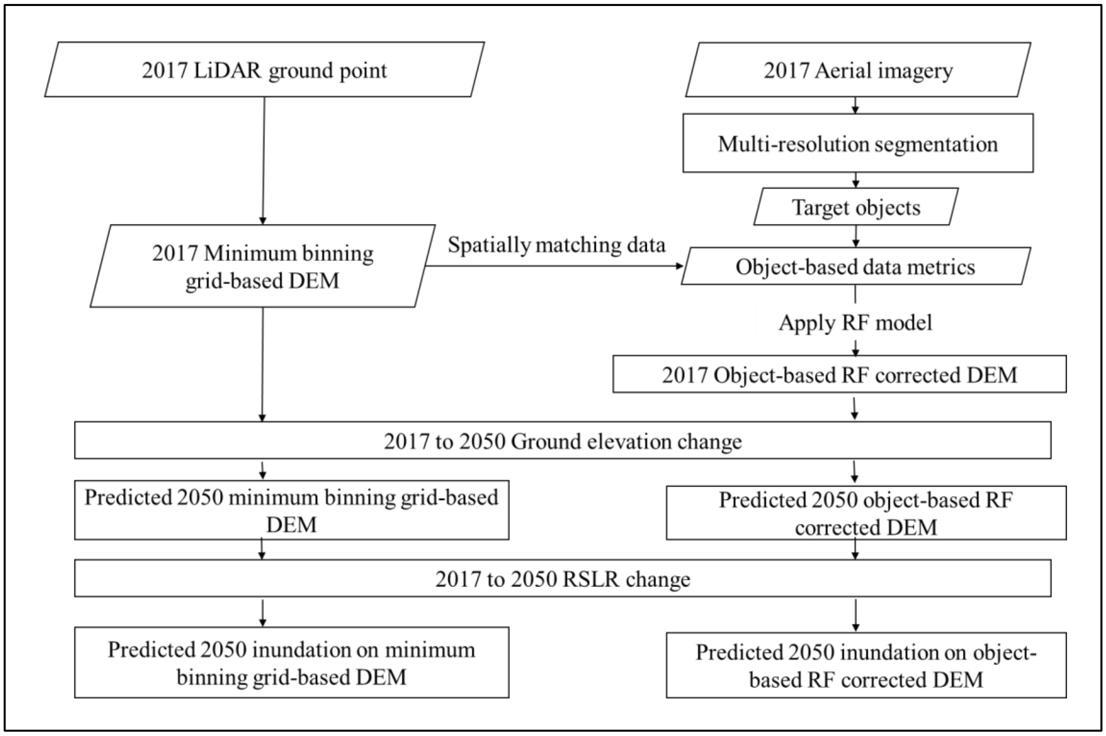

Figure 4.2 Framework for generating and comparing minimal binning and object-based RF DEM for a 2050 inundation map of coastal Louisiana.

4.3.1 Grid-based DEM and object-based RF corrected landscape model

The grid-based DEM was generated from utilizing the minimum binning interpolation technique to assign the minimal LiDAR point value to the grid as the ground elevation using the "LAS dataset to raster" tool in ArcGIS version 10.7.1 (https://www.esri.com/) toolbox, along with a void fill method to determine the value of cells that do not contain any LiDAR points. For further correction, the object-based RF corrected DEM was generated from the grid-based DEM raster data and aerial imagery. First, the image of 2017 Chenier Plain, Louisiana was segmented into image objects with scale 30. The "multiresolution segmentation algorithm" with scale 30 in eCognition Developer 9 was utilized to generate image objects based on spectral properties from the

NAIP NOAA 2017 4-band imagery. The grid-based minimum binning generated DEM raster data were spatially matched with each image object and statistical information was extracted by applying the "zonal statistics as table" tool to generate the statistics on each object for RF correction modeling. The information from each object included object square meters, center point longitude and latitude, the highest ground value, the average of the ground values, the lowest ground value, and the standard deviation of ground elevation. By applying the optimal RF corrected model in WEKA version 3.8 (Hall et al., 2009), the corrected ground elevation in each object polygon was generated and converted to the raster data in ArcGIS version 10.7.1 for the final DEM. For both the grid-based minimum binning generated DEM and the object-based RF corrected DEM, the 2017 base map was used to generate predicted 2050 DEM.

4.3.2 Ground elevation change model and RSLR inundation mapping

Unlike the traditional bathtub model that assumes the ground elevation remains the same over time, this study incorporates ground elevation change rates from 2007 to 2019 to predict the ground elevation in 2050. A time-series ground elevation model was utilized to forecast ground elevation to 2050 for a geographic position consistent with the CRMS monitoring sites in coastal Louisiana. Figure 4.3 shows the relationships between the multiple variables, including Ground Elevation Change (GEC), Surface Elevation Change (SEC), Vertical Accretion (VA), Shallow Subsidence (SS), Deep Subsidence (DS), Total Subsidence (TS), Global Sea Level Rise (GSLR), and RSLR. The VA, TS, SS, and DS define as downward positive; GSLR and RSLR define as upward positive. As shown in Figure 4.3, RSET-MH simultaneously can provide information on below-ground processes that influence ground elevation change. The difference between the rates of VA measured and SEC measured by RSET pin height can be attributed to processes occurring below the feldspar layer and above the bottom of the RSET rod as the SS (Equation 4.1) (Cahoon et al., 2002). On the other hand, the DS rate was estimated by solving the linear model equation as a function of the latitude of the CRMS monitoring site (Jankowski et al., 2017; Karegar et al., 2015). The sum of the SS rate and DS rate yielded the TS for each CRMS monitoring site (Equation 4.2). The ground elevation change results from interaction with total subsidence and vertical accretion, as shown in Equation 4.3.

Additionally, the change in RSLR results from the interaction with the change in the absolute elevation of the earth's ocean, as GSLR rate in the Gulf of Mexico is from 1992-2011 satellite altimetry data (2.4 mm per year) and local change (uplift or subsidence) with respect to the land surface (Jankowski et al., 2017). On the coast of Louisiana, the rate of RSLR was calculated for each CRMS monitoring station site by adding the present-day rate of GSLR in the Gulf of Mexico with ground elevation change, as shown in Equation 4.4. The predicted 2050 DEM could be represented by Equation 4.5, which uses DEM 2017 as a base map with 33 years (2017 to 2050) ground elevation change. Finally, the inundation area in 2050 is defined as Equation 4.6. Any predicted 2050 area that is not higher than the 33-year SLR is assumed to be inundated by 2050. Since this study uses the DEM 2017 as the base map, it assumes the DEM 2017 is not affected by RSLR.

$$Shallow\ subsidence = Vertical\ accretion - Surface\ elevation\ change$$

Equation 4.1

$$Total\ subsidence = Shallow\ subsidence + Deep\ subsidence$$

Equation 4.2

$$Ground\ elevation\ change =$$

$$VA - TS = VA - (SS + DS) = VA - (VA - SEC) + DS\ = SEC + DS$$

Equation 4.3

$$RSLR = GSLR - GEC$$ Equation 4.4

$$DEM\ 2050 = DEM\ 2017 + 33 * GEC$$ Equation 4.5

$$Inundation\ in\ 2050 = DEM\ 2050 - SL\ 2050 = DEM\ 2050 - 33 * GSLR$$

Equation 4.6

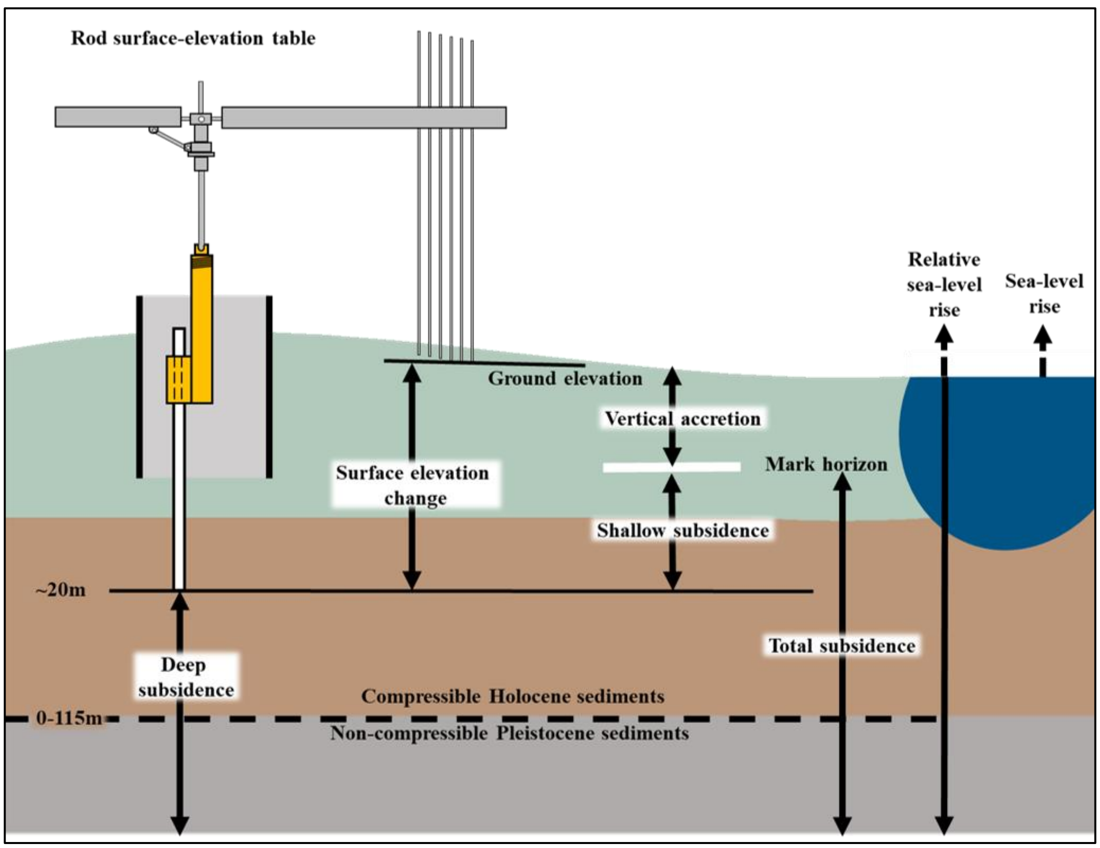

Figure 4.3 Relationship between SEC, VA, SS, DS, TS, SLR, and RSLR. Figure is not to scale. Modified from Jankowski et al., 2017.

4.4 Results

4.4.1 Ground elevation change rate

In order to predict the ground elevation in 2050, this study used simple linear regression of the association between the number of years and ground elevation measured by RSET from 2008 to 2018. The response variable is the ground elevation at each CRMS monitoring station, which was measured twice a year using the RSET technique, and the number of years (the initial year is 0) is the explanatory variable to account for predicting variation in the ground elevation change. Additionally, the number of years and ground elevation change scatterplots supplemented with a regression line were used to examine and gain insights for both the direction and strength of association and to best replicate modeling the relationship between time and ground elevation. The slope of the regression line is the regression coefficient, which is the absolute change of the line in the Y direction associated with an increase of one year in the X direction, and this number reveals how the ground elevation changes annually. For example, in Figure 4.4a, CRMS station 570 with a positive regression coefficient indicates that for each increasing year, the ground elevation increases by 0.017m. In Figure 4.4b, CRMS station 694 with a negative regression coefficient indicates that for each increasing year, the ground elevation decreases by 0.024 m. The slope provides an idea of showing how much of the points are positive increase as the time goes by, and how many of them are negative change as time goes by. As shown in Equation 4.3, the final ground elevation change incorporates the deep subsidence rate though the monitoring years.

A histogram showing ground elevation regression coefficients for all 127 CRMS monitoring stations is shown in Figure 4.5a; interpolation of ground elevation change rates on the Chenier Plain, LA using Inverse Distance Weighted (IDW) methods in ArcGIS version 10.7.1 is shown in Figure 4.5b. The IDW is a commonly used interpolation method that determines cell value using a linearly weighted combination of a set of nearby point values and assumes the ground elevation change influence decreases with distance increase. The blue area in Figure 4.5b represents the ground elevation rate with a negative value, indicating the area is annually losing ground elevation. The largest decrease in ground elevation is around 16.23 mm per year (Figure 4.5a). More than 60% of ground elevation change rate is around 0 to 9 mm per year, shown as green and yellow color in Figure 4.5b, while the highest ground elevation change is around 9 to 23 mm per year, shown as red.

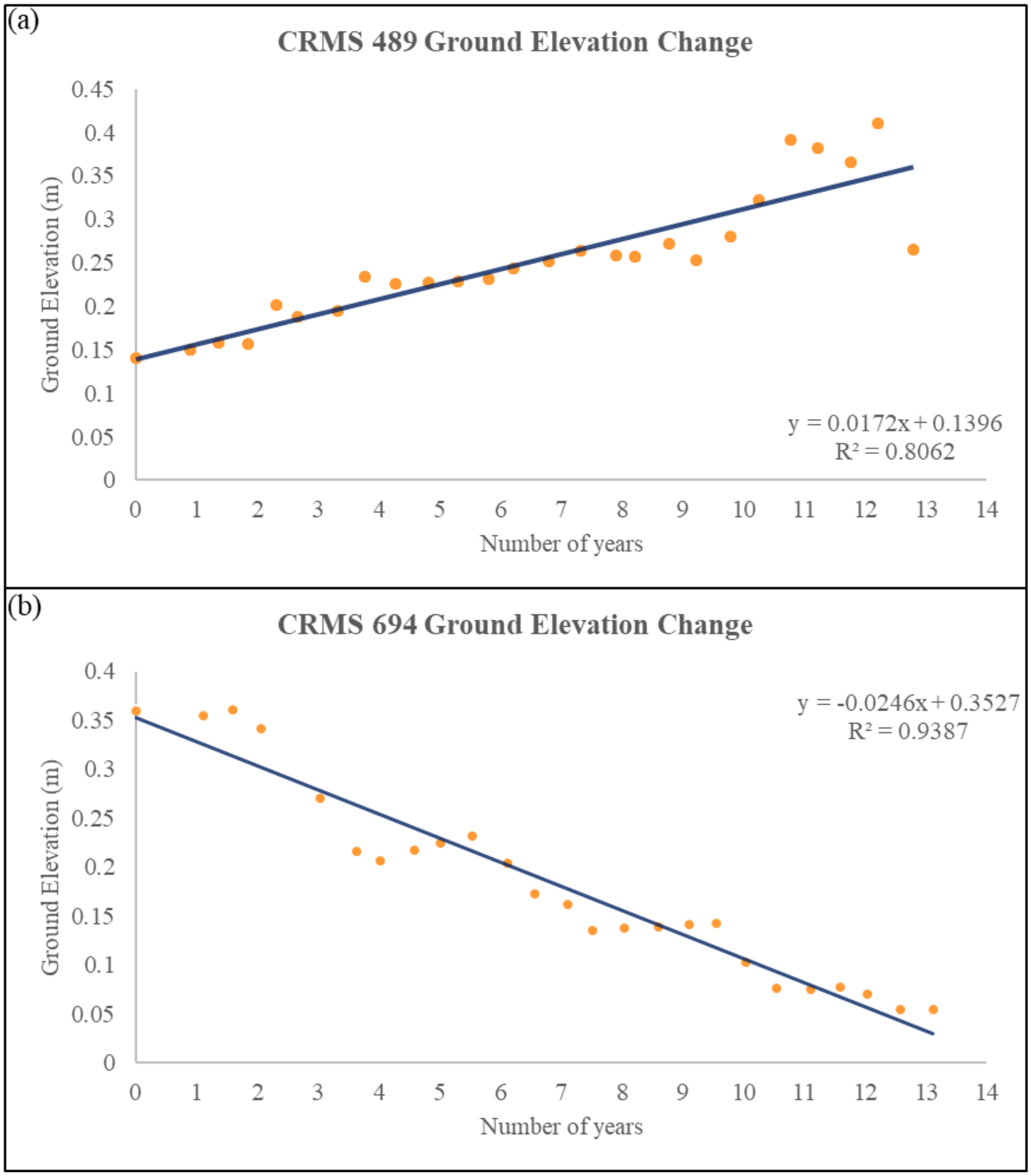

Figure 4.4 Example of relationship between ground elevation change and number of years: (a) a strong positive relationship; (b) a strong negative relationship.

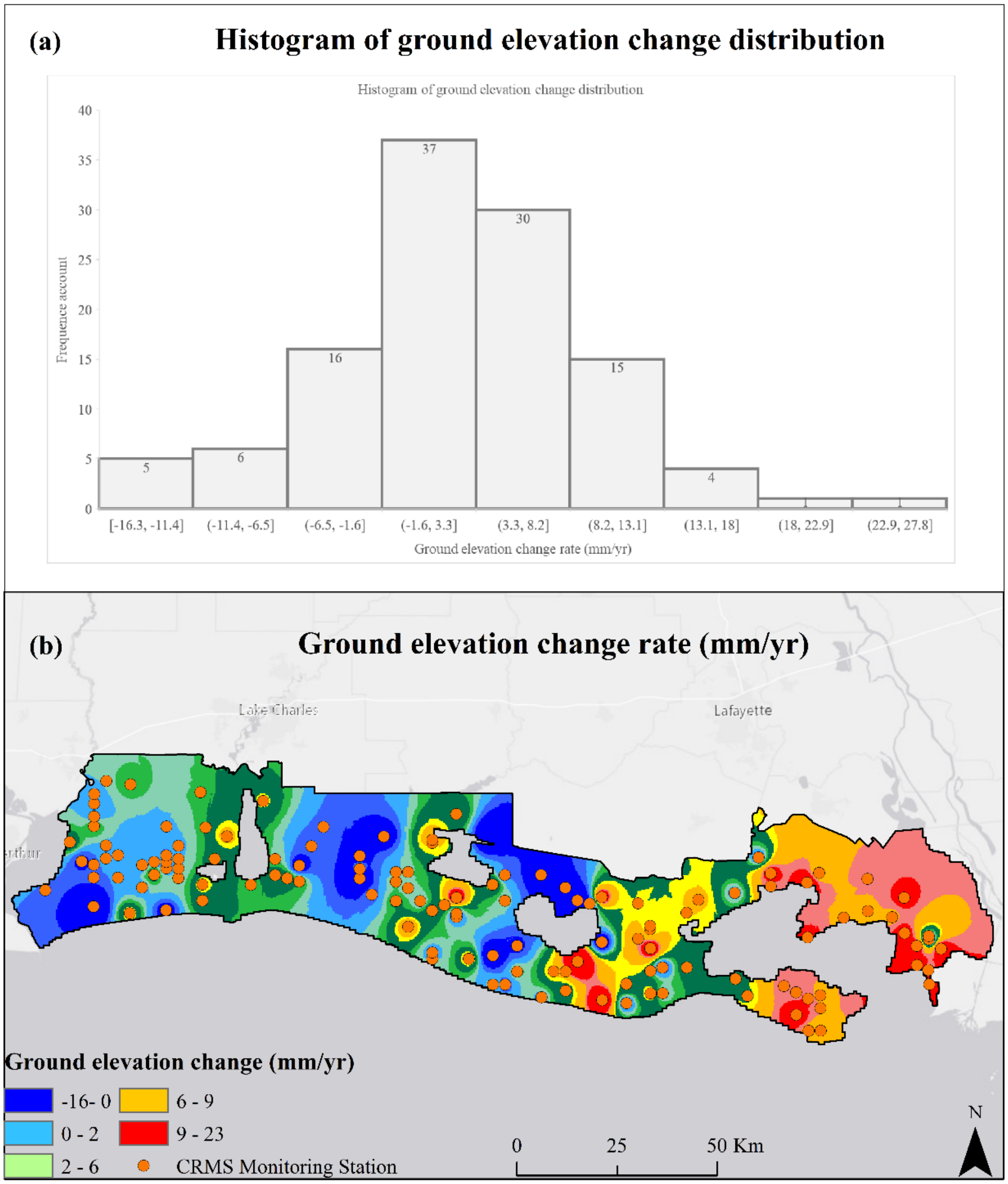

Figure 4.5 Histogram showing distribution of ground elevation change rates (a); Interpolated rate of ground elevation change in Chenier Plain, Louisiana (b).

4.4.2 Predicting 2050 grid-based DEM and object-based corrected DEM

The DEM based on LiDAR point elevation data collected in 2017 was used as the base map for the landscape modeling in 2050 and mapping inundation area due to RSLR. Figure 4.6a presents 2017 grid-based DEM generated with minimum binning interpolation technique. For further correction, Figure 4.6b shows 2017 object-based RF corrected DEM. Blue color in Figure 4.6 represents the ground elevation below the NAVD 88 vertical datum, while green represents ground elevation above ground under 0.37 m. Yellow and orange colors represent wetland ground elevation from 0.37 to 0.77 m, while pink to dark red represent ground elevation 0.77 to 25.32 m above NAVD vertical datum. Grid-based minimum binning DEM generally show a relatively higher ground elevation compared to object-based RF corrected DEM. Both 2017 grid-based DEM and object-based RF corrected DEM are used for the 2017 landscape base map.

The predicted 2050 DEM were generated by applying ground elevation change rate raster on both the grid-based 2017 DEM base map and the object-based RF corrected 2017 DEM base map using Equation 4.5. Figure 4.7a shows the predicted 2050 grid-based DEM and Figure 4.7b shows the object-based RF corrected DEM on the Chenier Plain, Louisiana. Blue color in Figure 4.7 represents the ground elevation below the NAVD 88 vertical datum, while green, yellow, and red represent ground elevation above ground.

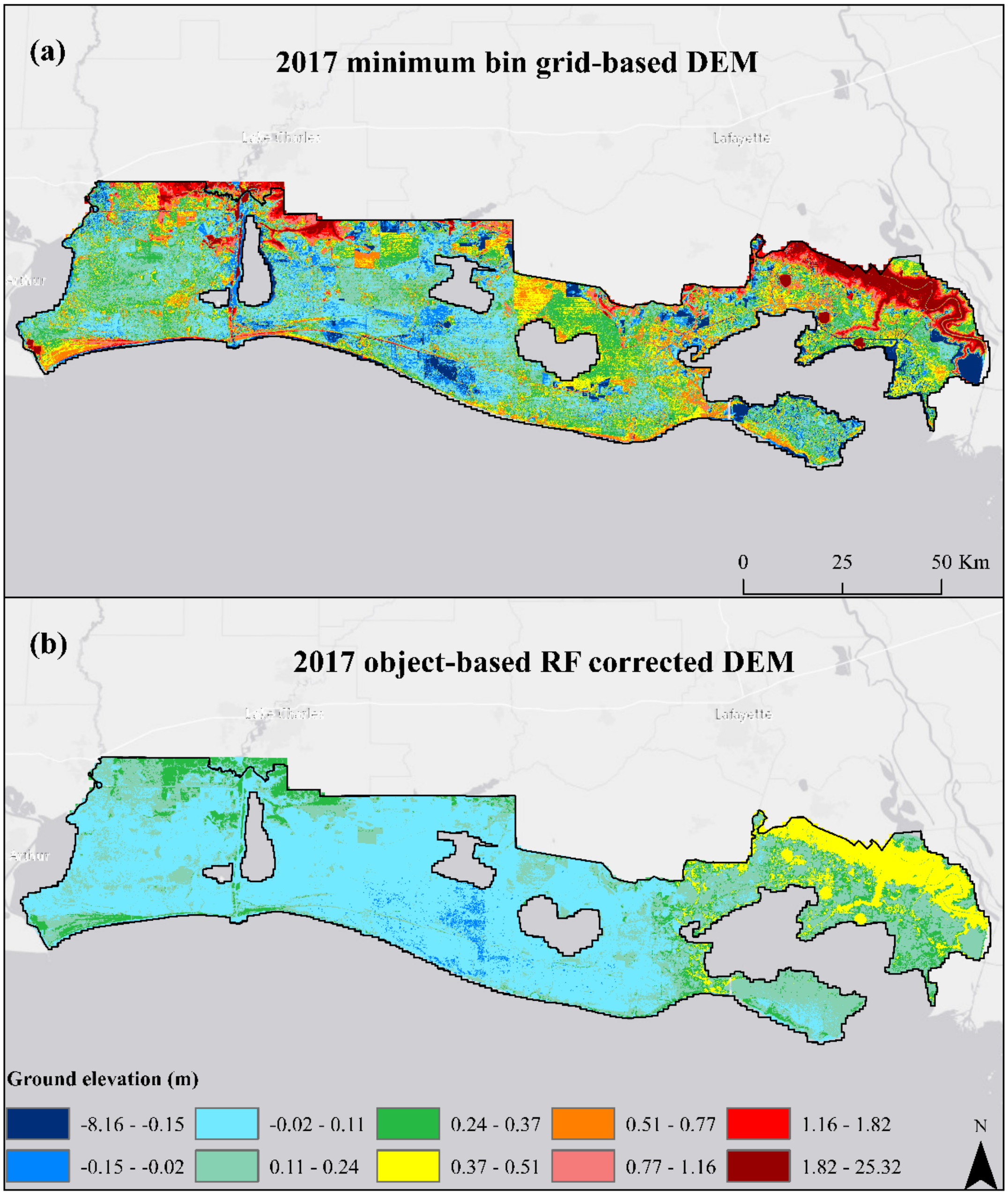

Figure 4.6 2017 DEM: (a) grid-based minimal binning DEM; (b) object-based RF corrected DEM.

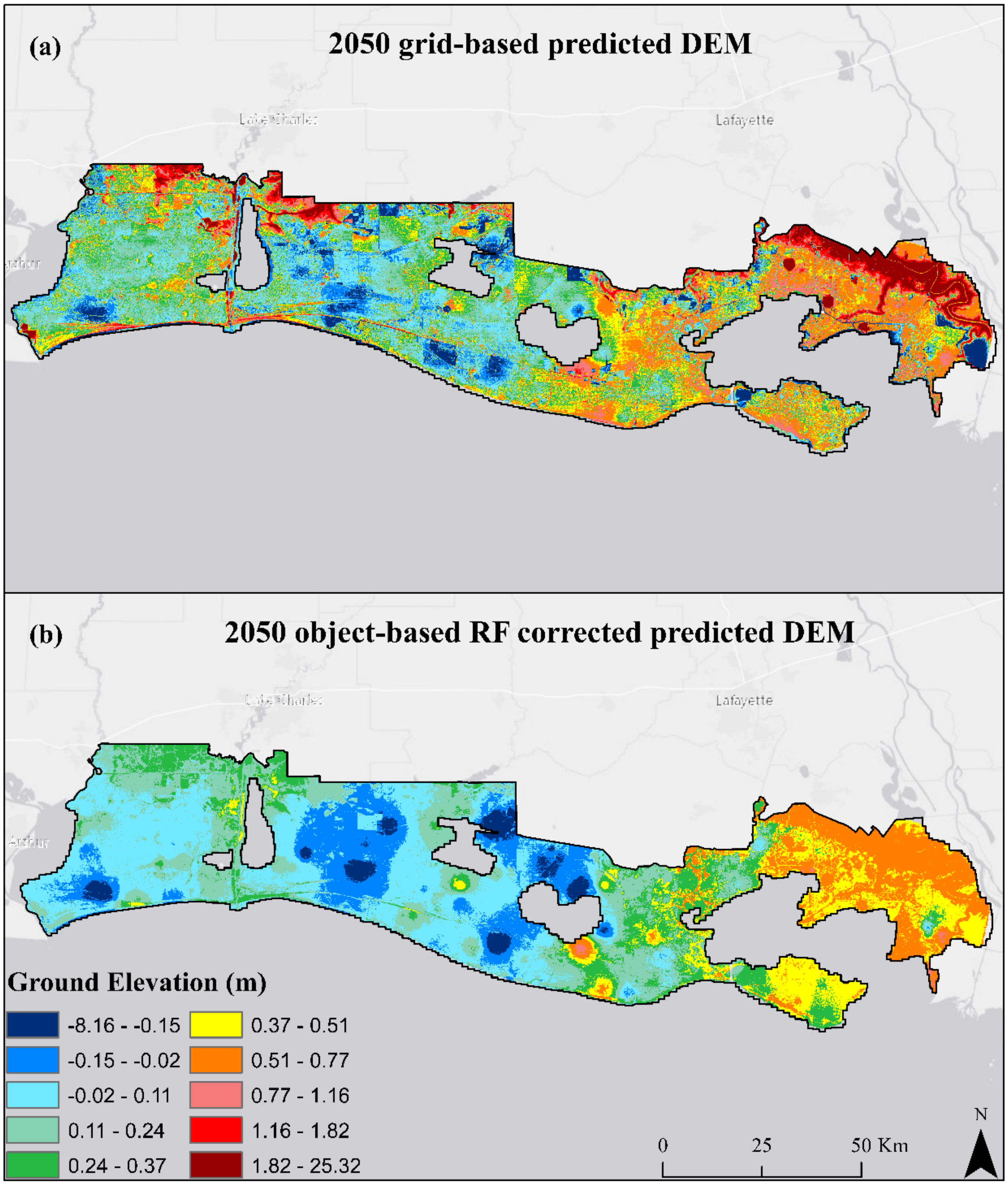

Figure 4.7 Predicted DEM in 2050: (a) grid-based predicted DEM; (b) object-based RF corrected predicted DEM.

4.4.3 Mapping RSLR inundation in 2050

In order to model 2050 inundation area due to RSLR in Chenier Plain, Louisiana, any areas that are below the SLR change are assumed to be flooded in 2050 in this study. The predicted 2050 grid-based minimum binning DEM and object-based RF corrected DEM were applied as the predicted DEM to quantify inundation area with GSLR change by Equation 4.6. In ArcGIS 10.7.1, both grid-based minimal binning and object-based RF corrected predicted 2050 DEM raster data subtract the GSLR change from 2017 to 2050. If the area is not as high as the GSLR, the result shows a negative value and assumes that the area will be underwater by the year 2050. The area which will be underwater is shown by red color in Figure 4.8.

There is a significant difference between predicted inundation on grid-based minimum binning generated DEM and object-based RF corrected DEM. Figure 4.8a shows the inundation area with 2050 grid-based minimum binning predicted DEM as 1567 km^2, which is 20% of the area of the entire Chenier Plain, Louisiana. On the other hand, Figure 4.8b shows the inundation area due to RSLR as 2620 km^2, 34% of the entire Chenier Plain, Louisiana. The results show that the applied object-based RF corrected DEM has great promise in remote sensing applications. Grids in grid-based DEM are arbitrary units and can contain mixed signals from surrounding areas. For coastal wetland ecosystems, the high heterogeneity of land cover and spectral similarity of plant species often leads to “salt and pepper” effects. On the other hand, applying object-based corrected DEM merge pixels into objects and correct LiDAR-derived DEM at the object level to optimize within-pixel homogeneity and without-pixel heterogeneity.

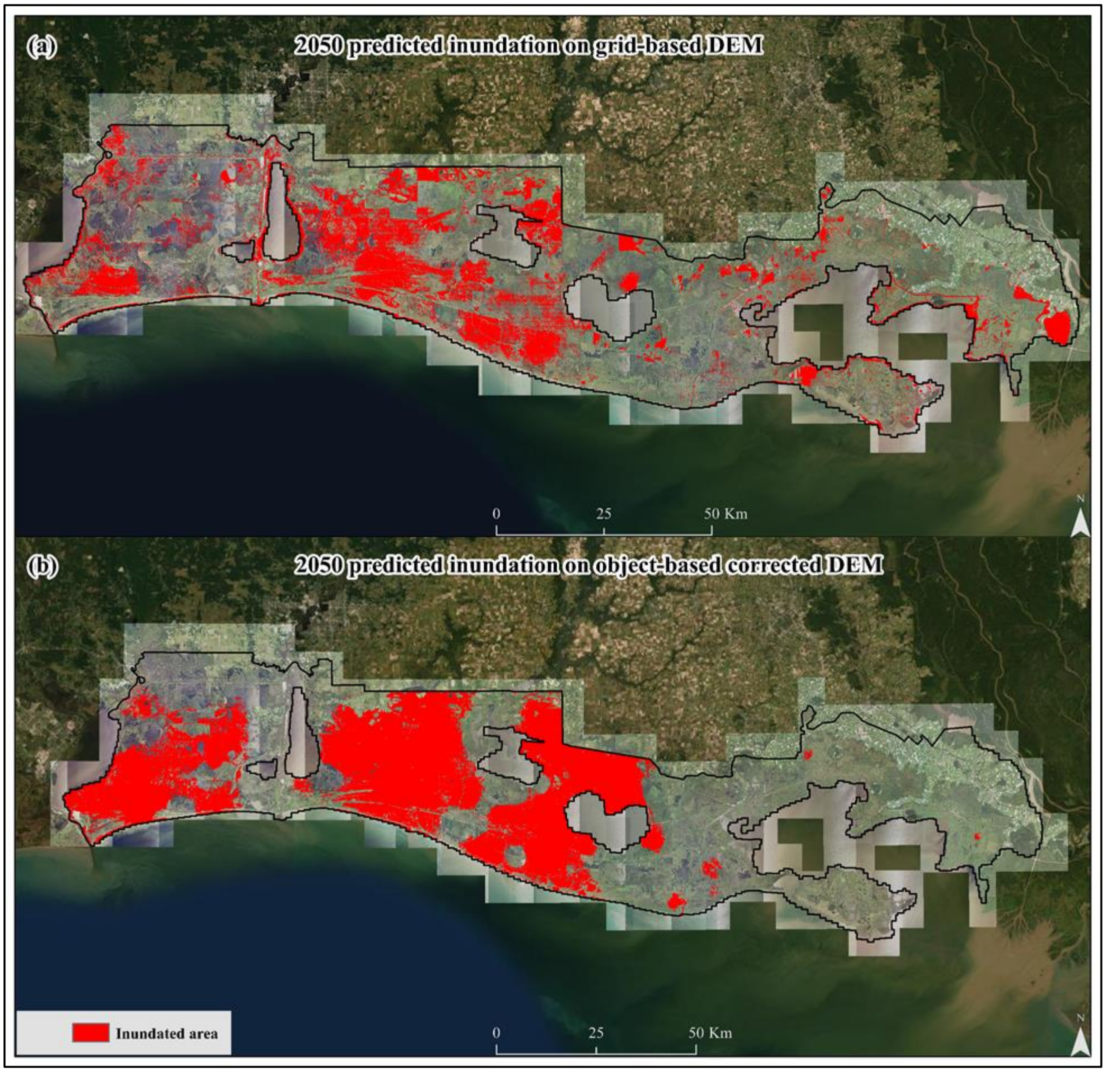

Figure 4.8 Predicted inundation area in 2050 in Chenier Plain, Louisiana: (a) 2050 inundation area with grid-based minimum binning predicted DEM; (b) 2050 inundation area with object-based RF corrected predicted DEM.

4.5 Discussion

4.5.1 Relative sea-level rise modeling

Typically, SLR inundation analysis uses tide gauges. However, tide gauge data are inherently measuring SLR relative to the anchor point, which in coastal Louisiana might be a few tens of meters below the land surface (Jankowski et al., 2017). Considering the high shallow subsidence in coastal Louisiana, tide gauges in this region are not able to capture precise RSLR. This study applied the method from Jankowski et al. (2017) to calculate the RSLR concerning the land surface for each individual site by adding an estimate of the deep subsidence rate and observed shallow subsidence on top of the GSLR. This provides an essential improvement for meaningful understanding of the response of coastal wetlands in Louisiana to RSLR. The deep subsidence rates are generated from solving the linear model equation as a function of latitude from the study of Karegar et al. (2015). Meanwhile, the shallow subsidence rate was calculated from field data as the difference between vertical accretion minus the ground elevation change. The sum of shallow subsidence and deep subsidence yielded the total subsidence for each CRMS monitoring station. Finally, the mean rate of SLR (2.0 ± 0.4 mm per year) in the Gulf of Mexico from 1992 to 2011 was calculated from satellite altimetry data in a previous study (Letetrel et al., 2015). Thus, this study calculated the rate of RSLR for each CRMS monitoring station to predict water levels in 2050.

The results of this study show that 34% of the entire Chenier Plain, Louisiana will be impacted by RSLR by 2050, which is different from the results of Jankowski et al. (2017) who showed that 58% of the CRMS sites in the Chenier Plain could not keep pace with RSLR. The difference between these studies may be due to two main reasons. First, the results from this study were generated from 2017 corrected DEM that applied the ground elevation change annually increased to 2050 DEM. On the other hand, the study from Jankowski et al. (2017) compared the ground elevation change rate with the RSLR rate, so any site where the RSLR rate exceeds the rate of SEC is considered vulnerable to the RSLR. However, the study from Kirwan et al., 2008 shows that some marshes are vulnerable to SLR and get submerged even their vertical accretion rates are higher than the rates of the RSLR. Since identifying RSLR as the primary driver of wetland loss is a complicated process. If the initial wetland ground elevation is relatively low, this area will experience more frequently inundated and have more sediment deposited, which results in a relatively high vertical accretion rate (Fagherazzi et al., 2012). On the other hand, if the wetland ground elevation is relatively high, the inundation from the tide is relatively low, the accretion is slow (Fagherazzi et al., 2012). Second, the study from Jankowski et al. (2017) analyzes the vertical accretion rate and RSLR rate on a point based on CRMS monitoring station. This study examines the wetland inundation on a regional scale with applied object-based LiDAR-derived DEM as a regional scale 3D terrain surface model.

4.5.2 Uncertainty of future RSLR and ground elevation change

In this study, the ground elevation change rate has generated from a time-series model and utilized to forecast ground elevation to 2050 at each CRMS monitoring station, by using simple linear regression using the ground elevation from 2008 to 2018 measured by RSET as a function of the number of years. The slop of the regression line was used to examine the direction and ground elevation changes annually. Some monitoring station ground elevation changes are highly related to the number of years.

For example, monitoring station number 489 and 694 with R^2 over 0.8 in Figure 4.4. However, there are some monitoring stations the ground elevation change is not highly related to the number of years. As the result showing in chapter 2, the ground elevation change is a complex process and is related to various environmental variables. For forecasting the DEM in 2050, this study simplified the impact of environmental variables on ground elevation and applied the regression coefficient from ground elevation change with the number of years from 2008 to 2018 as the ground elevation change rate.

Although this model included a vital feedback mechanism between RSLR and vertical ground elevation change, this study did not consider other climate change that may further enhance the adaptability of coastal wetlands to RSLR. The developed RSLR inundation model projected no net loss in wetland extent under the RSLR by 2050, but there are still uncertainties in future years about the capacity of natural ecosystems to self-regulate to perturbations. Additionally, ground elevation change in coastal wetlands is a complex procedure impacted by numerous environmental drivers. For example, although SLR can increasing flooding frequency and duration, which triggers vegetation mortality and soil collapse, studies have shown higher frequency and longer flooding duration have positive impacts on sediment accumulation and several plant productivity (Kirwan et al., 2012; Morris et al., 2002). Additionally, Tonelli et al. (2010) found that when the marsh is flooded, the wave effect from hurricanes on wetlands boundaries is less. Moreover, Mariotti et al. (2010) demonstrated that a low rate of SLR increases wave dissipation and sediment deposition.

Human impact on coastal wetlands ecosystems, especially the increased atmospheric carbon dioxide concentrations by global warming enhanced photosynthesis and plant productivity of wetland species will impact accumulation of plant organic matter, which is a primary process controlling wetland vertical development (Rogers et al., 2015). Additionally, warmer temperatures improve coastal wetland vegetation productivity, which has been experimentally demonstrated to further ground elevation change; for example, Kirwan et al. (2009) estimated that an increase of 4°C could boost productivity by up to 40%. Together, these ecogeomorphic interactions allow marshes to adapt to SLR (Baustian et al., 2012; Morris et al., 2002). Even the most robust vertical accretion models may underestimate the potential for coastal wetlands to adapt to SLR, and that makes prediction of future sustainability difficult (Langley et al., 2009)

4.6 Conclusion

The main aim of this study was to provide a high vertical accuracy relative sea-level inundation map of coastal Louisiana. By achieving this goal, this study developed a robust approach to modeling and mapping RSLR inundation by combining LiDAR point data and RF corrected models with high accuracy DEM products. This study draws the following conclusions:

1) Instead of traditionally applying the SLR rate on DEM, this study chose RSLR by combining the mean rate of SLR in the Gulf of Mexico from 1992 to 2011 satellite altimetry data (2.0 ± 0.4 mm per year) with site-specific subsidence rates (including shallow subsidence and deep subsidence). Compared with most previous studies that have relied on SLR measured by tide gauges, the RSLR in coastal Louisiana used in this study better captures the full amount of RSLR.

2) The object-based RF corrected DEM is an attractive alternative to the traditional grid-based minimum binning generated DEM. By incorporating multispectral

aerial imagery and applying the OBIA technique correcting the LiDAR ground elevation on object-based with RF correct model, which significantly approved the vertical accuracy of LiDAR-derived DEM.

3) By predicting the RSLR inundation by 2050, consider the ground elevation change by applied ground elevation change rate generated from over ten years of RSET ground elevation observation. The results show that the grid-based minimum binning corrected DEM was overestimating the capability on RSLR impact compared with the object-based RF corrected DEM.

CHAPTER 5: SUMMARY AND CONCLUSION

This dissertation identified and quantified environmental variables that characterize coastal wetland ground elevation, improved LiDAR terrain measurements, and analyzed inundation by linking terrain changes with RSLR using the ten-year RSET field measurements large-scale LiDAR data. Forecasting the impact of RSLR on wetland environments generally involves dynamic models that account for ongoing processes such as vertical migration and sediment accretion. In addition, the RSLR impact model requires high-resolution DEM with the vertical error should be at least twice as certain as the SLR increment (NOAA, 2010), which is difficult to achieve with most open-source LiDAR data. The result of this study provides a robust model for LiDAR correction approach using high accuracy RSET and consider the ground elevation change (vertical accretion and subsidence) while predicting the inundation by RSLR offers an opportunity to assist with wetlands conservation, preservation, and restoration in coastal Louisiana.

The long-term survival of the coastal wetlands depended on if their ground elevation change rate is equally or higher than the rising sea level rate (Morris et al., 2002). Several external forces, like wetland vegetation, hydrology, and distance to the sediment source, have a substantial impact on vertically building ground elevation (Mariotti and Fagherazzi, 2010). In 2006, the CRMS established a network station for effectively monitoring the progress of restoration projects in coastal Louisiana. More than a decade of hydrology, vegetation, and ground elevation data measured by RSET techniques have been simultaneously collected to date. The size and density of this data provide an unprecedented opportunity for studying coastal wetland ground elevation dynamics along with how different environmental variables shape the terrain in coastal Louisiana. Although RSET techniques have been popularly used for monitoring and modeling in coastal wetlands, the previous studies have focused on the qualitative analysis of how environmental variables impact ground elevation (Krauss et al., 2008). Limited and scarce quantitative analysis exists, e.g., Roger et al. (2012) explored linear modeling techniques to quantify the contribution of climatic, hydrological, and site-specific factors to ground elevation dynamics. However, due to the complicated processes involved in sediment elevation change, the linear regression cannot adequately explain the relationship. Therefore, more quantitative analysis based on testing nonlinear relationship interplay between ground elevation and environment variables is necessary.

The chapter 2 examined three machine learning algorithms (RF, SVM, and ANN) and MLR for evaluating the statistical relationship between ground elevation change and environmental variables. This study presents a broad overview of quantifying the formation and evolution of coastal wetlands under different environmental variables. In particular, this study focused on applying machine learning algorithms to quantify nonlinear feedback between environmental variables and ground elevation from 2008 to 2018 across the entire coastal Louisiana wetlands, and shed light on the long-term evolution and resilience of coastal wetland systems. A ground elevation dynamic model considering ground elevation data from 2008 to 2018 as functions of environmental variables incorporates all the mechanisms that influence ground elevation, including hydrological variables, vegetation variables, and site-specific variables derived from the CRMS network in Louisiana. This study designed a robust approach that evaluated MLR and three machine learning regression models, including RF, SVM, and ANN. Machine learning techniques are effective at generating accurate ground elevation models from environment variables. The RF model achieved the best accuracy (r = 0.74 and RMSE = 10.8 cm). Since the wetland ecosystem is the manifestation of complex ecological and physical interactions, the numerical model provides an opportunity to capture the nonlinear between environmental variables and the ground elevation change process and shed light on the long-term wetland evolution and resilience the SLR.

The primary input for SLR impact models requires a high-resolution DEM, typically produced using LiDAR data. However, high vegetation density wetlands require inputs of a higher vertical accuracy DEM in order to meet NOAA recommended that the vertical error of a DEM should be at least twice as certain as the SLR increment (NOAA, 2010). Previous studies of increasing accuracy of LiDAR-derived DEM have primarily focused on using field technology real-time kinematic (RTK) to enhance the integrity of LiDAR products in the wetland environments (e.g., Hladik et al., 2012; McClure et al., 2016; Montané et al., 2006). Although RTK has vertical accuracy approximately 0.02 to 0.12 m (Renschler et al., 2002), the limited spatial distribution still hinders the comparability from using RTK correcting LiDAR data across a regional space (McClure et al., 2016). Although the study has shown that combining RTK and LiDAR data reduced the DEM mean error from 0.16 meter to 0.04 meter, annual rates of SLR and wetlands sediment surface elevation operate on a millimeter scale, using RTK is correcting LiDAR data will exceed the accuracy requirement for SLR vulnerability assessment (McClure et al., 2016). Moreover, SLR affects coastal-wide landscaped wetlands; the limited spatial distribution RTK in a relatively small area hinders the comparability from using RTK correcting LiDAR data across a regional space (McClure et al., 2016). On the other hand, there are approximately 390 site monitoring stations (Fig.1.1) that use RSET techniques to measure ground elevation in a large scale covering entire coastal Louisiana with a higher vertical accuracy of 0.0010 to 0.0015 m (Cahoon et al., 2002). With the broader spatial distribution of RSET and high vertical accuracy, it is expected that RSET will have a better performance than RTK in reducing the vertical error of LiDAR-derived DEM in Louisiana coastal wetlands.

There have been several technological advancements recently to improve LiDAR-derived elevations including minimum bin gridding method to filter and classify LiDAR last return signals (e.g., Medeiros et al., 2015; Schmid et al., 2011; Wang et al., 2009; Töyrä et al., 2003); subtraction of species-specific bias based on vegetation cover maps (e.g., Hladik and Alber, 2012; Hladik et al., 2013; McClure et al., 2016); and using full-waveform LiDAR data with nonparametric modeling techniques. Little effort has been put for correcting LiDAR data at objects based on machine learning algorithms. Several studies have confirmed that OBIA in conjunction with machine learning techniques can produce higher accuracies for mapping and modeling the coastal wetland ecosystem (Zhang and Xie, 2012; Zhang et al., 2013; Zhang and Xie, 2014; Zhang et al., 2016; Zhang et al., 2018a; Zhang et al., 2018b). Thus, this study developed an object-based correction approach for high vertical accuracy DEM by integrating LiDAR point data, aerial imagery, and RSET. OBIA considers the spectral and spatial characteristics of surrounding pixels and incorporates similar pixels into a homogeneous image object instead of the grid-based methods used in previous studies that may mix signals from surrounding areas. This study has confirmed that OBIA, in conjunction with machine learning techniques, can produce high accuracy for correcting LiDAR-derived DEM in coastal wetlands ecosystems. Overall, this study combined data fusions of LiDAR point data, field measured RSET, and aerial imagery with robust machine learning algorithms for improving vertical accuracy of LiDAR-derived DEM from RMSE 0.355 to 0.008 m and achieved the best result with the r = 0.83 for ground elevation estimation for coastal wetlands in Louisiana. The data fusion approach using 2017 LiDAR point data, aerial photography, field ground elevation data measured by RSET, and machine learning algorithms was promising for generating a high vertical accuracy DEM. Although the study areas' location is different, these results are comparable with the study by Copper et al., (2018) and Roger et al. (2018) that nonparametric machine learning modeling techniques are powerful for ground elevation estimation, especially the RF model.

Studies of the long-term observation of coastal wetlands stability and maintenances conclude that wetland ground elevation must have the ability to adjust to changes in rates of SLR (Friedrichs and Perry, 2001). The simplest SLR impact model, referred to as the bathtub model, is an elevation-based model that assumes land area adjacent to the sea and below a given water elevation is inundated (Gesch, 2009). This model only requires a DEM and water level as input and can be used to rapidly determine the area at risk (Roger et al., 2012). However, the current bathtub model solely takes rising water into account, without considering the changing of the ground elevation change. Forecasting the impact of SLR on wetland environmental generally involves more dynamic models that account for ongoing processes such as vertical accretion, shallow, and deep subsidence. This study applied the corrected DEM and considered the ground elevation change and subsidence which not only provided ways to increase the integrity of SLR inundation assessments but also presented the results in a way that is easily communicated to the general public. To assess the ground elevation change, over ten years ground elevation generated from CRMS monitoring station using RSET technique was analyzed for generating the ground elevation change rate. The ground elevation rate and RSLR rate were applied to both the 2017 grid-based minimum binning DEM and the object-based RF corrected DEM and annually increased to 2050. There is a significant difference between the 2050 RSLR inundation area between grid-based minimum binning DEM and object-based RF corrected DEM. The inundation area with 2050 grid-based minimum binning predicted DEM as 1567 km^2, which is 20% of the entire Chenier Plain, Louisiana. On the other hand, the inundation area due to RSLR with 2050 using object-based RF corrected predicted DEM as 2620 km^2 which is 34% of the whole Chenier Plain, Louisiana. The results show the grid-based has overestimated the capability on RSLR impact compare with the object-based RF corrected DEM.

With large amounts of coastal wetlands being converted to open water in Louisiana, the remaining land concerns will persist while facing the highest rates of RSLR in the world (Jankowski et al., 2017). The study of how environmental variables impact ground elevation change is crucial for analyzing and modeling the response of the rising sea level impact on wetland ecosystem. Additionally, fusing remote sensing data with RSET field data in object-based analysis provides the unique opportunity to enhance confidence for assessment of coastal wetland conservation, preservation, and restoration. Finally, the higher spatial coverage is in high demand for managers, especially as wetland restoration efforts increase to mitigate the impacts of the high rate of RSLR.

REFERENCES

Adam, P., 1990. Saltmarsh Ecology. Cambridge University Press, Cambridge, UK.

Agatonovic-Kustrin, S., & Beresford, R. (2000). Basic concepts of artificial neural network (ANN) modeling and its application in pharmaceutical research. *Journal of Pharmaceutical and Biomedical Analysis*, *22*(5), 717–727. https://doi.org/10.1016/S0731-7085(99)00272-1

Barbier, E. B., Hacker, S. D., Kennedy, C., Koch, E. W., Stier, A. C., & Silliman, B. R. (2011). The value of estuarine and coastal ecosystem services. *Ecological Monographs*, *81*(2), 169–193. https://doi.org/10.1890/10-1510.1

Baustian, J. J., Mendelssohn, I. A., & Hester, M. W. (2012). Vegetation's importance in regulating surface elevation in a coastal salt marsh facing elevated rates of sea level rise. *Global Change Biology*, *18*(11), 3377–3382. https://doi.org/10.1111/j.1365-2486.2012.02792.x

Benz, U. C., Hofmann, P., Willhauck, G., Lingenfelder, I., & Heynen, M. (2004). Multi-resolution, object-oriented fuzzy analysis of remote sensing data for GIS-ready information. *ISPRS Journal of Photogrammetry and Remote Sensing*, *58*(3–4), 239–258. https://doi.org/10.1016/j.isprsjprs.2003.10.002

Blaschke, T. (2010). Object based image analysis for remote sensing. *ISPRS Journal of Photogrammetry and Remote Sensing*, *65*(1), 2–16. https://doi.org/10.1016/j.isprsjprs.2009.06.004

Blum, M. D., & Roberts, H. H. (2009). Drowning of the Mississippi Delta due to insufficient sediment supply and global sea-level rise. *Nature Geoscience*, *2*(7), 488–491. https://doi.org/10.1038/ngeo553

Boesch, D. F., Josselyn, M. N., Mehta, A. J., Morris, J. T., Nuttle, W. K., Simenstad, C. A., & Swift, D. J. P. (1994). Scientific Assessment of coastal wetland loss, restoration and management in Louisiana. *Coastal Research*, i–v, 1–103.

Bourennane, H., Couturier, A., Pasquier, C., Chartin, C., Hinschberger, F., Macaire, J.-J., & Salvador-Blanes, S. (2014). Comparative performance of classification algorithms for the development of models of spatial distribution of landscape structures. *Geoderma*, *219–220*, 136–144. https://doi.org/10.1016/j.geoderma.2014.01.001

Breiman L (2001) Random forests. *Machine Learning*, *45*(1), 5–32.

Bricker-Urso, S., Nixon, S. W., Cochran, J. K., Hirschberg, D. J., & Hunt, C. (1989). Accretion Rates and Sediment Accumulation in Rhode Island Salt Marshes. *Estuaries*, *12*(4), 300. https://doi.org/10.2307/1351908

Brovelli, M. A., Cannata, M., & Longoni, U. M. (2004). LIDAR Data Filtering and DTM Interpolation Within GRASS. *Transactions in GIS*, *8*(2), 155–174. https://doi.org/10.1111/j.1467-9671.2004.00173.x

Buffington, K. J., Dugger, B. D., Thorne, K. M., & Takekawa, J. Y. (2016). Statistical correction of LiDAR-derived digital elevation models with multispectral airborne imagery in tidal marshes. *Remote Sensing of Environment*, *186*, 616–625. https://doi.org/10.1016/j.rse.2016.09.020

Cadol, D., Engelhardt, K., Elmore, A., & Sanders, G. (2014). Elevation-dependent surface elevation gain in a tidal freshwater marsh and implications for marsh persistence. *Limnology and Oceanography*, *59*(3), 1065–1080. https://doi.org/10.4319/lo.2014.59.3.1065

Cahoon, D. R. (1995). Relationships among marsh surface topography, hydroperiod, and soil accretion in a deteriorating Louisiana salt marsh. *Journal of Coastal Research*, *11*(2), 15.

Cahoon, D. R. (2006). A review of major storm impacts on coastal wetland elevations. *Estuaries and Coasts*, *29*(6), 889–898. https://doi.org/10.1007/BF02798648

Cahoon, D. R., Lynch, J. C., Hensel, P., Boumans, R., Perez, B. C., Segura, B., & Day, J. W. (2002a). High-precision measurements of wetland sediment elevation: I. Recent improvements to the sedimentation-erosion table. *Journal of Sedimentary Research*, *72*(5), 730–733. https://doi.org/10.1306/020702720730

Cahoon, D. R., Lynch, J. C., Perez, B. C., Segura, B., Holland, R. D., Stelly, C., Stephenson, G., & Hensel, P. (2002b). High-precision measurements of wetland sediment elevation: II. The rod surface elevation table. *Journal of Sedimentary Research*, *72*(5), 734–739. https://doi.org/10.1306/020702720734

Cahoon, D. R., Reed, D. J., & Day, J. W. (1995). Estimating shallow subsidence in microtidal salt marshes of the southeastern United States: Kaye and Barghoorn revisited. *Marine Geology*, *128*(1–2), 1–9. https://doi.org/10.1016/0025-3227(95)00087-F

Cheng Wang, Menenti, M., Stoll, M.-P., Feola, A., Belluco, E., & Marani, M. (2009). Separation of ground and low vegetation signatures in LiDAR measurements of salt-marsh environments. *IEEE Transactions on Geoscience and Remote Sensing*, *47*(7), 2014–2023. https://doi.org/10.1109/TGRS.2008.2010490

Chmura, G. L., & Hung, G. A. (2004). Controls on salt marsh accretion: A test in salt marshes of Eastern Canada. *Estuaries*, *27*(1), 70–81. https://doi.org/10.1007/BF02803561

Coleman, Harry H. Roberts, & Gregory W. Stone. (1998). Mississippi River Delta: An Overview. *Journal of Coastal Research*, *14*(3), 698–716.

Cooper, H. M., Zhang, C., Davis, S. E., & Troxler, T. G. (2019). Object-based correction of LiDAR DEM using RTK-GPS data and machine learning modeling in the coastal Everglades. *Environmental Modelling & Software*, *112*, 179–191. https://doi.org/10.1016/j.envsoft.2018.11.003

Costanza, R., de Groot, R., Sutton, P., van der Ploeg, S., Anderson, S. J., Kubiszewski, I., Farber, S., & Turner, R. K. (2014). Changes in the global value of ecosystem services. *Global Environmental Change*, *26*, 152–158. https://doi.org/10.1016/j.gloenvcha.2014.04.002

Couvillion, B. R., Beck, H., Schoolmaster, D., & Fischer, M. (2017). *Land area change in coastal Louisiana (1932 to 2016)*. 26.

Criminisi, A., Shotton, J., Konukoglu, E., (2011). Decision forests: A unified framework for classification, regression, density estimation, manifold learning and semi-supervised learning. *Found. Trends Comput. Graph*. Vis. 7 (2–3), 81–227.

Day, J. W., Boesch, D. F., Clairain, E. J., Kemp, G. P., Laska, S. B., Mitsch, . . . Whigham, D. F. (2007). Restoration of the Mississippi Delta: Lessons from

Hurricanes Katrina and Rita. *Science*, *315*(5819), 1679–1684. https://doi.org/10.1126/science.1137030

Day, J. W., Britsch, L. D., Hawes, S. R., Shaffer, G. P., Reed, D. J., & Cahoon, D. (2000). Pattern and process of land loss in the Mississippi Delta: A spatial and temporal analysis of wetland habitat change. *Estuaries*, *23*(4), 425. https://doi.org/10.2307/1353136

DeLaune, R. D., Whitcomb, J. H., Patrick, W. H., Pardue, J. H., & Pezeshki, S. R. (1989). Accretion and canal impacts in a rapidly subsiding wetland. I. 137 Cs and 210 Pb techniques. *Estuaries*, *12*(4), 247. https://doi.org/10.2307/1351904

Drăguţ L, Csillik O, Eisank C, Tiede D (2014) Automated parameterisation for multi-scale image segmentation on multiple layers. *ISPRS Journal of Photogrammetry and Remote Sensing* 88: 119–127.

Dronova, I. (2015). Object-based image Analysis in wetland research: A review. *Remote Sensing*, *7*(5), 6380–6413. https://doi.org/10.3390/rs70506380

Eberly L. E. (2007). Multiple linear regression. In Ambrosius W. T. (Ed.), *Topics in biostatistics. Methods in molecular biology*™ (Vol. 404). Totowa, NJ: Humana Press.

Fagherazzi, S., Carniello, L., D'Alpaos, L., & Defina, A. (2006). Critical bifurcation of shallow microtidal landforms in tidal flats and salt marshes. *Proceedings of the National Academy of Sciences*, *103*(22), 8337–8341. https://doi.org/10.1073/pnas.0508379103

Fagherazzi, S., Kirwan, M. L., Mudd, S. M., Guntenspergen, G. R., Temmerman, S., D'Alpaos, A., . . . Clough, J. (2012). Numerical models of salt marsh evolution:

Ecological, geomorphic, and climatic factors. *Reviews of Geophysics*, *50*(1), RG1002. https://doi.org/10.1029/2011RG000359

Feagin, R. A., Lozada-Bernard, S. M., Ravens, T. M., Moller, I., Yeager, K. M., & Baird, A. H. (2009). Does vegetation prevent wave erosion of salt marsh edges? *Proceedings of the National Academy of Sciences*, *106*(25), 10109–10113. https://doi.org/10.1073/pnas.0901297106

Fisher, P. F., & Tate, N. J. (2006). Causes and consequences of error in digital elevation models. *Progress in Physical Geography*, *30*(4), 467–489. https://doi.org/10.1191/0309133306pp492ra

Fisk HN, McFarlan E Jr (1955) Late quaternary deltaic deposits of the Mississippi River. Geol Soc Am Spec Pap 62:279–302

Folse, T. M., Sharp, L. A., West, J. L., Hymel, M. K., Troutman, P., McGinnis, T. E., . . . Miller, C. M. (2018). *A Standard Operating Procedures Manual for the Coastwide Reference Monitoring System-Wetlands: Methods for Site Establishment, Data Collection, and Quality Assurance/Quality Control.* Louisiana Coastal Protection and Restoration Authority. Baton Rouge, LA. 226 pp.

Friedman, J. H. (2002). Stochastic gradient boosting. *Computational Statistics & Data Analysis*, *38*(4), 367–378. https://doi.org/10.1016/S0167-9473(01)00065-2

Friedrichs, C. T., & Perry, J. E. (2001). Tidal salt marsh morphodynamics: A synthesis. *Journal of Coastal Research*, *27*, 33.

Friess, D. A., Krauss, K. W., Horstman, E. M., Balke, T., Bouma, T. J., Galli, D., & Webb, E. L. (2012). Are all intertidal wetlands naturally created equal? Bottlenecks, thresholds and knowledge gaps to mangrove and saltmarsh ecosystems. *Biological Reviews*, *87*(2), 346–366. https://doi.org/10.1111/j.1469-185X.2011.00198.x

Friedrichs, C. T., and J. E. Perry (2001), Tidal salt marsh morphodynamics. *J. Coastal Res.*, 27, 6–36.

Gedan, K. B., Kirwan, M. L., Wolanski, E., Barbier, E. B., & Silliman, B. R. (2011). The present and future role of coastal wetland vegetation in protecting shorelines: Answering recent challenges to the paradigm. *Climatic Change*, *106*(1), 7–29. https://doi.org/10.1007/s10584-010-0003-7

Gesch, D. B. (2009). Analysis of LiDAR elevation data for improved identification and delineation of lands vulnerable to sea-level rise. *Journal of Coastal Research*, *10053*, 49–58. https://doi.org/10.2112/SI53-006.1

Göpfert, J., & Heipke, C. (2006). Assessment of LiDAR DTM Accuracy in Coastal Vegetated Areas Int Arch Photogram Remote Sens Spat Inf Sci 36:79–85

Hall, M., Frank, E., Holmes, G., Pfahringer, B., Reutemann, P., & Witten, I. H. (2009). The WEKA data mining software: An update. *ACM SIGKDD Explorations Newsletter*, *11*(1), 10–18. https://doi.org/10.1145/1656274.1656278

Hall C, Tharakan P, Hallock J, Cleveland C, Jefferson M. Hydrocarbons and the evolution of human culture [published correction appears in Nature. 2004 Jan 8;427(6970):175]. Nature. 2003;426(6964):318-322. doi:10.1038/nature02130

Hastie, T., Tibshirani, R., & Friedman, J. (2013). *The elements of statistical learning: Data mining, inference, and prediction*. Springer Science & Business Media.

Hladik, C., & Alber, M. (2012). Accuracy assessment and correction of a LIDAR-derived salt marsh digital elevation model. *Remote Sensing of Environment*, *121*, 224–235. https://doi.org/10.1016/j.rse.2012.01.018

Hladik, C., Schalles, J., & Alber, M. (2013). Salt marsh elevation and habitat mapping using hyperspectral and LIDAR data. *Remote Sensing of Environment*, *139*, 318–330. https://doi.org/10.1016/j.rse.2013.08.003

Hodgson, M. E., & Bresnahan, P. (2004). Accuracy of airborne LiDAR-derived elevation: empirical assessment and error budget. *Photogrammetric Engineering*, 10.

Hopkinson, C., Chasmer, L. E., Sass, G., Creed, I. F., Sitar, M., Kalbfleisch, W., & Treitz, P. (2005). Vegetation class dependent errors in LiDAR ground elevation and canopy height estimates in a boreal wetland environment. *Canadian Journal of Remote Sensing*, *31*(2), 16.

Howes, N. C., FitzGerald, D. M., Hughes, Z. J., Georgiou, I. Y., Kulp, M. A., Miner, M. D., . . . Barras, J. A. (2010). Hurricane-induced failure of low salinity wetlands. *Proceedings of the National Academy of Sciences*, *107*(32), 14014–14019. https://doi.org/10.1073/pnas.0914582107

Huang C, Davis LS, Townshend JRG (2002) An assessment of support vector machines for land cover classification. International Journal of Remote Sensing 23(4): 725–749.

Jankowski, K. L., Törnqvist, T. E., & Fernandes, A. M. (2017). Vulnerability of Louisiana’s coastal wetlands to present-day rates of relative sea-level rise. *Nature Communications*, *8*(1), 14792. https://doi.org/10.1038/ncomms14792

Jensen JR (2015) *Introductory Digital Image Processing: A Remote Sensing Perspective*, 4th ed., Prentice Hall Series in Geographic Information Science.

Karegar, M. A., Dixon, T. H., & Malservisi, R. (2015). A three-dimensional surface velocity field for the Mississippi Delta: Implications for coastal restoration and flood potential. *Geology*, *43*(6), 519–522. https://doi.org/10.1130/G36598.1

Kesel, R. H. (1988). The decline in the suspended load of the Lower Mississippi River and its influence on adjacent wetlands. Environmental Geology and Water Sciences, 11(3), 271–281. https://doi.org/10.1007/BF02574816

Kirwan, M.L., Murray, A.B., 2007. A coupled geomorphic and ecological model of tidal marsh evolution. Proceedings of the National Academy of Sciences 104, 6118–6122.

Kirwan, M. L., & Guntenspergen, G. R. (2012). Feedbacks between inundation, root production, and shoot growth in a rapidly submerging brackish marsh: MARSH ROOT GROWTH UNDER SEA LEVEL RISE. *Journal of Ecology*, *100*(3), 764–770. https://doi.org/10.1111/j.1365-2745.2012.01957.x

Kirwan, M. L., Guntenspergen, G. R., & Morris, J. T. (2009). Latitudinal trends in *Spartina alterniflora* productivity and the response of coastal marshes to global change. *Global Change Biology*, *15*(8), 1982–1989. https://doi.org/10.1111/j.1365-2486.2008.01834.x

Kirwan, M. L., & Megonigal, J. P. (2013). Tidal wetland stability in the face of human impacts and sea-level rise. *Nature*, *504*(7478), 53–60. https://doi.org/10.1038/nature12856

Kirwan, M. L., Temmerman, S., Skeehan, E. E., Guntenspergen, G. R., & Fagherazzi, S. (2016). Overestimation of marsh vulnerability to sea level rise. *Nature Climate Change*, *6*(3), 253–260. https://doi.org/10.1038/nclimate2909

Krauss, K. W., Lovelock, C. E., McKee, K. L., López-Hoffman, L., Ewe, S. M. L., & Sousa, W. P. (2008). Environmental drivers in mangrove establishment and early development: A review. *Aquatic Botany*, *89*(2), 105–127. https://doi.org/10.1016/j.aquabot.2007.12.014

Kuhn M, Wing J, Weston S, Williams A, Keefer C, Engelhardt A (2016) Caret: Classification and regression training. Retrieved from: https://CRAN.R-project.org/package=caret (accessed 20 January 2020).

Kulawardhana, R. W., Popescu, S. C., & Feagin, R. A. (2014). Fusion of LiDAR and multispectral data to quantify salt marsh carbon stocks. *Remote Sensing of Environment*, *154*, 345–357. https://doi.org/10.1016/j.rse.2013.10.036

Langley, J. A., McKee, K. L., Cahoon, D. R., Cherry, J. A., & Megonigal, J. P. (2009). Elevated CO2 stimulates marsh elevation gain, counterbalancing sea-level rise. *Proceedings of the National Academy of Sciences*, *106*(15), 6182–6186. https://doi.org/10.1073/pnas.0807695106

Lefsky, M. A., Cohen, W. B., Harding, D. J., Parker, G. G., Acker, S. A., & Gower, S. T. (2002). LiDAR remote sensing of above-ground biomass in three biomes. *Global Ecology and Biogeography*, *11*(5), 393–399. https://doi.org/10.1046/j.1466-822x.2002.00303.x

Leonard, L. A. (1997). Controls of sediment transport and deposition in an incised mainland marsh basin, southeastern North Carolina. *Wetlands*, *17*(2), 263–274. https://doi.org/10.1007/BF03161414

Leonard, L. A., & Luther, M. E. (1995). Flow hydrodynamics in tidal marsh canopies. *Limnology and Oceanography*, *40*(8), 1474–1484. https://doi.org/10.4319/lo.1995.40.8.1474

Letetrel, C., Karpytchev, M., Bouin, M.-N., Marcos, M., SantamarÍa-Gómez, A., & Wöppelmann, G. (2015). Estimation of vertical land movement rates along the coasts of the Gulf of Mexico over the past decades. *Continental Shelf Research*, *111*, 42–51. https://doi.org/10.1016/j.csr.2015.10.018

Li, Z., Zhu, Q., & Gold, C. (2005). *Digital terrain modeling: Principles and methodology*. CRC Press.

Liu, X., Zhang, Z., Peterson, J., & Chandra, S. (2008). *Large Area DEM Generation Using Airborne LiDAR Data and Quality Control*. 7.

Lynch, J. C., P. Hensel, and D. R. Cahoon. 2015. The surface elevation table and marker horizon technique: A protocol for monitoring wetland elevation dynamics. *Natural Resource Report NPS/NCBN/NRR*—2015/1078. National Park Service, Fort Collins, Colorado.

Mas JF and Flores JJ (2008) The application of artificial neural networks to the analysis of remotely sensed data. *International Journal of Remote Sensing 29:* 617–663.

Marani, M., D'Alpaos, A., Lanzoni, S., Carniello, L., & Rinaldo, A. (2007). Biologically-controlled multiple equilibria of tidal landforms and the fate of the Venice lagoon. *Geophysical Research Letters*, *34*(11). https://doi.org/10.1029/2007GL030178

Marani, M., Lanzoni, S., Silvestri, S., & Rinaldo, A. (2004). Tidal landforms, patterns of halophytic vegetation and the fate of the lagoon of Venice. *Journal of Marine Systems*, *51*(1–4), 191–210. https://doi.org/10.1016/j.jmarsys.2004.05.012

Mariotti, G., & Fagherazzi, S. (2010). A numerical model for the coupled long-term evolution of salt marshes and tidal flats. *Journal of Geophysical Research*, *115*(F1), F01004. https://doi.org/10.1029/2009JF001326

Maxwell, A. E., Warner, T. A., & Fang, F. (2018). Implementation of machine-learning classification in remote sensing: An applied review. *International Journal of Remote Sensing*, *39*(9), 2784–2817. https://doi.org/10.1080/01431161.2018.1433343

McClure, A., Liu, X., Hines, E., & Ferner, M. C. (2016). Evaluation of Error Reduction Techniques on a LIDAR-Derived Salt Marsh Digital Elevation Model. *Journal of Coastal Research*, *318*, 424–433. https://doi.org/10.2112/JCOASTRES-D-14-00185.1

McKee, K. L., Cahoon, D. R., & Feller, I. C. (2007). Caribbean mangroves adjust to rising sea level through biotic controls on change in soil elevation. *Global Ecology and Biogeography*, *16*(5), 545–556. https://doi.org/10.1111/j.1466-8238.2007.00317.x

Medeiros, S., Hagen, S., Weishampel, J., & Angelo, J. (2015). Adjusting LiDAR-Derived Digital Terrain Models in Coastal Marshes Based on Estimated Aboveground Biomass Density. *Remote Sensing*, *7*(4), 3507–3525. https://doi.org/10.3390/rs70403507

Mendelssohn, I. A., & Morris, J. T. (2000). Eco-Physiological Controls on the Productivity of Spartina Alterniflora Loisel. *Concepts and Controversies in Tidal Marsh Ecology*, 59–80. doi: 10.1007/0-306-47534-0_5

Moeslund, J. E., Arge, L., Bøcher, P. K., Nygaard, B., & Svenning, J.-C. (2011). Geographically Comprehensive Assessment of Salt-Meadow Vegetation-Elevation Relations Using LiDAR. *Wetlands*, *31*(3), 471–482. https://doi.org/10.1007/s13157-011-0179-2

Montané, J. M., & Torres, R. (2006). Accuracy Assessment of LiDAR Saltmarsh Topographic Data Using RTK GPS. *Photogrammetric Engineering & Remote Sensing*, *72*(8), 961–967. https://doi.org/10.14358/PERS.72.8.961

Morris, J. T. (2006). Competition among marsh macrophytes by means of geomorphological displacement in the intertidal zone. *Estuarine, Coastal and Shelf Science*, *69*(3–4), 395–402. https://doi.org/10.1016/j.ecss.2006.05.025

Morris, J. T., Sundareshwar, P. V., Nietch, C. T., Kjerfve, B., & Cahoon, D. R. (2002). Responses of Coastal Wetlands to Rising Sea Level. *Ecology*, *83*(10), 2869–2877. https://doi.org/10.1890/0012-9658(2002)083[2869:ROCWTR]2.0.CO;2

Mountrakis, G., Im, J., & Ogole, C. (2011). Support vector machines in remote sensing: A review. *ISPRS Journal of Photogrammetry and Remote Sensing*, *66*(3), 247–259. https://doi.org/10.1016/j.isprsjprs.2010.11.001

Mudd, S. M., D'Alpaos, A., & Morris, J. T. (2010). How does vegetation affect sedimentation on tidal marshes? Investigating particle capture and hydrodynamic controls on biologically mediated sedimentation. *Journal of Geophysical Research*, *115*(F3), F03029. https://doi.org/10.1029/2009JF001566

Nicholls, R. J., & Cazenave, A. (2010). Sea-Level Rise and Its Impact on Coastal Zones. *Science*, *328*(5985), 1517–1520. https://doi.org/10.1126/science.1185782

National Oceanic and Atmospheric Administration (NOAA), 2010. Technical Considerations for Use of Geospatial Data in Sea Level Change Mapping and Assessment. Silver Spring, Maryland: U.S. Department of Commerce, NOAA NOS Technical Report, NOAA National Ocean Service, 141p. http://www.csc.noaa.gov/ digitalcoast/_/pdf/SLC_Technical_Considerations_Document.pdf.

Nyman, J. A., Walters, R. J., Delaune, R. D., & Patrick, W. H. (2006). Marsh vertical accretion via vegetative growth. *Estuarine, Coastal and Shelf Science*, *69*(3–4), 370–380. https://doi.org/10.1016/j.ecss.2006.05.041

Nyman, J., DeLaune, R., Roberts, H., & Patrick, W. (1993). Relationship between vegetation and soil formation in a rapidly submerging coastal marsh. *Marine Ecology Progress Series*, *96*, 269–279. https://doi.org/10.3354/meps096269

Owen, D. E. (2008). Geology of the Chenier Plain of Cameron Parish, southwestern Louisiana. In *Geological Society of America Field Guide 14, 2008 Joint Annual Meeting, Houston, Texas, 5–9 October 2008* (pp. 27–38). Geological Society of America. https://doi.org/10.1130/2008.fld014(02)

Pal, M., & Mather, P. M. (2003). An assessment of the effectiveness of decision tree methods for land cover classification. *Remote Sensing of Environment*, *86*(4), 554–565. https://doi.org/10.1016/S0034-4257(03)00132-9

Palmer, M. R., Nepf, H. M., Pettersson, T. J. R., & Ackerman, J. D. (2004). Observations of particle capture on a cylindrical collector: Implications for particle accumulation and removal in aquatic systems. *Limnology and Oceanography*, *49*(1), 76–85. https://doi.org/10.4319/lo.2004.49.1.0076

Perry, C. L., & Mendelssohn, I. A. (2009). Ecosystem effects of expanding populations of Avicennia germinans in a Louisiana salt marsh. *Wetlands*, *29*(1), 396–406. https://doi.org/10.1672/08-100.1

Populus, J., Barreau, G., Faxilleau, J., Kerdreux, M., L'Yavanc, J., 2001. Assessment of the Lidar topographic technique over a coastal area. In: Proceedings of Coast-GIS'01: 4th International Symposium on GIS and Computer Mapping for Coastal Zone Management, Halifax, Nova Scotia, p. 11.

Rahmstorf, S. (2010). A new view on sea level rise. *Nature Reports Climate Change*, *1004*, 44–45. https://doi.org/10.1038/climate.2010.29

Reed, D. J. (ED.). 1995. Status and historical rrends of hydrologic modification, reduction in sediment availability, and habitat Loss/modification in the Barataria and Terrebonne Estuarine System. *Barataria-Terrebonne National Estuary Program Publication* No. 20, Thibodeaux, Louisiana.

Renschler, C. S., Flanagan, D. C., Engel, B. A., Kramer, L. A. & Sudduth, K. A. (2002). Site-specific decision-making based on RTK-GPS survey and six alternative elevation data sources: Watershed topography and delineation. *Trans*. *ASAE* 45, 1883–1895

Rogers, J. N., Parrish, C. E., Ward, L. G., & Burdick, D. M. (2016). Assessment of Elevation Uncertainty in Salt Marsh Environments using Discrete-Return and Full-Waveform LiDAR. *Journal of Coastal Research, 76,* 107–122. https://doi.org/10.2112/SI76-010

Rogers, J. N., Parrish, C. E., Ward, L. G., & Burdick, D. M. (2018). Improving salt marsh digital elevation model accuracy with full-waveform LiDAR and nonparametric predictive modeling. *Estuarine, Coastal and Shelf Science*, *202*, 193–211. https://doi.org/10.1016/j.ecss.2017.11.034

Rogers, K., Saintilan, N., & Copeland, C. (2012). Modelling wetland surface elevation dynamics and its application to forecasting the effects of sea-level rise on estuarine wetlands. *Ecological Modelling*, *244*, 148–157. https://doi.org/10.1016/j.ecolmodel.2012.06.014

Rogers, K., & Woodroffe, C. D. (2015). Tidal Flats and Salt Marshes. In G. Masselink & R. Gehrels (Eds.), *Coastal Environments and Global Change* (pp. 227–250). John Wiley & Sons, Ltd. https://doi.org/10.1002/9781119117261.ch10

Rosso, P. H., Ustin, S. L., & Hastings, A. (2006). Use of LiDAR to study changes associated with Spartina invasion in San Francisco Bay marshes. *Remote Sensing of Environment*, *100*(3), 295–306. https://doi.org/10.1016/j.rse.2005.10.012

Rybczyk, J. M., & Cahoon, D. R. (2002). Estimating the potential for submergence for two wetlands in the Mississippi River Delta. *Estuaries*, *25*(5), 985–998. https://doi.org/10.1007/BF02691346

Schile, L. M., Callaway, J. C., Morris, J. T., Stralberg, D., Parker, V. T., & Kelly, M. (2014). Modeling Tidal Marsh Distribution with Sea-Level Rise: Evaluating the Role of Vegetation, Sediment, and Upland Habitat in Marsh Resiliency. *PLoS ONE*, *9*(2), e88760. https://doi.org/10.1371/journal.pone.0088760

Schmid, K. A., Hadley, B. C., & Wijekoon, N. (2011). Vertical Accuracy and Use of Topographic LIDAR Data in Coastal Marshes. *Journal of Coastal Research*, *275*, 116–132. https://doi.org/10.2112/JCOASTRES-D-10-00188.1

Schmidt, K. S., & Skidmore, A. K. (2003). Spectral discrimination of vegetation types in a coastal wetland. *Remote Sensing of Environment*, *85*(1), 92–108. https://doi.org/10.1016/S0034-4257(02)00196-7

Stagg, C.L., Sharp, L.A., McGinnis, T.E., and Snedden, G.A., (2013). Submergence Vulnerability Index development and application to Coastwide Reference Monitoring System Sites and Coastal Wetlands Planning, Protection and Restoration Act projects: *U.S. Geological Survey Open-File Report* 2013–1163, 12 p., http://pubs.usgs.gov/of/2013/1163/.

Steyer, G. D., Sasser, C. E., Visser, J. M., Swenson, E. M., Nyman, J. A., & Raynie, R. C. (2003). A Proposed Coast-Wide Reference Monitoring System for Evaluating Wetland Restoration Trajectories in Louisiana. In B. D. Melzian, V. Engle, M. McAlister, S. Sandhu, & L. K. Eads (Eds.), *Coastal Monitoring through Partnerships* (pp. 107–117). Springer Netherlands. https://doi.org/10.1007/978-94-017-0299-7_11

Stralberg, D., Brennan, M., Callaway, J. C., Wood, J. K., Schile, L. M., Jongsomjit, D., Kelly, M., Parker, V. T., & Crooks, S. (2011). Evaluating Tidal Marsh Sustainability in the Face of Sea-Level Rise: A Hybrid Modeling Approach Applied to San Francisco Bay. *PLoS ONE*, *6*(11), e27388. https://doi.org/10.1371/journal.pone.0027388

Streutker, D. R., & Glenn, N. F. (2006). LiDAR measurement of sagebrush steppe vegetation heights. *Remote Sensing of Environment*, *102*(1–2), 135–145. https://doi.org/10.1016/j.rse.2006.02.011

Swanson, K. M., Drexler, J. Z., Schoellhamer, D. H., Thorne, K. M., Casazza, M. L., Overton, C. T., Callaway, J. C., & Takekawa, J. Y. (2014). Wetland Accretion Rate Model of Ecosystem Resilience (WARMER) and Its Application to Habitat Sustainability for Endangered Species in the San Francisco Estuary. *Estuaries and Coasts*, *37*(2), 476–492. https://doi.org/10.1007/s12237-013-9694-0

Temmerman, S., Moonen, P., Schoelynck, J., Govers, G., & Bouma, T. J. (2012). Impact of vegetation die-off on spatial flow patterns over a tidal marsh: Tidal Marsh Die-Off and Flow Patterns. *Geophysical Research Letters*, *39*(3), n/a-n/a. https://doi.org/10.1029/2011GL050502

Tonelli, M., Fagherazzi, S., & Petti, M. (2010). Modeling wave impact on salt marsh boundaries. *Journal of Geophysical Research*, *115*(C9), C09028. https://doi.org/10.1029/2009JC006026

Töyrä, J., Pietroniro, A., Hopkinson, C., & Kalbfleisch, W. (2003). Assessment of airborne scanning laser altimetry (LiDAR) in a deltaic wetland environment. *Canadian Journal of Remote Sensing*, *29*(6), 718–728. https://doi.org/10.5589/m03-040

Trimble (2017) eCognition Developer 9.0.1 Reference Book, Trimble GmnH Munich Germany.

Turner, R. E., Baustian, J. J., Swenson, E. M., & Spicer, J. S. (2006). Wetland Sedimentation from Hurricanes Katrina and Rita. *Science*, *314*(5798), 449–452. https://doi.org/10.1126/science.1129116

Wang C., Menenti, M., Stoll, M.-P., Feola, A., Belluco, E., & Marani, M. (2009). Separation of Ground and Low Vegetation Signatures in LiDAR Measurements of Salt-Marsh Environments. IEEE Transactions on Geoscience and Remote Sensing, 47(7), 2014–2023. https://doi.org/10.1109/TGRS.2008.2010490

Webb, E. L., Friess, D. A., Krauss, K. W., Cahoon, D. R., Guntenspergen, G. R., & Phelps, J. (2013). A global standard for monitoring coastal wetland vulnerability to accelerated sea-level rise. *Nature Climate Change*, *3*(5), 458–465. https://doi.org/10.1038/nclimate1756

Webster, T., & Lemckert, C. (2002). Sediment resuspension within a microtidal estuary/embayment and the implication to channel management. *Journal of Coastal Research*, *36*, 753–759. https://doi.org/10.2112/1551-5036-36.sp1.753

Zhang C, Mishra DR, Penning S (2019) Mapping salt marsh soil properties using imaging spectroscopy. *ISPRS Journal of Photogrammetry and Remote Sensing* 148: 221-234.

Zhang C, Denka S, Cooper H, Mishra DR (2018a) Quantification of sawgrass marsh aboveground biomass in the coastal Everglades using object-based ensemble analysis and Landsat data. *Remote Sensing of Environment* 204: 366–379.

Zhang C, Denka S, Mishra DR (2018b) Mapping freshwater marsh species in the wetlands of Lake Okeechobee using very high-resolution aerial photography and lidar data. *International Journal of Remote Sensing* 39: 5600–5618.

Zhang C, Selch D, Cooper H (2016) A framework to combine three remotely sensed data sources for vegetation mapping in the Central Florida Everglades. *Wetlands* 36(2): 201–213.

Zhang C and Xie X (2014) Data fusion and classifier ensemble techniques for vegetation mapping in the coastal Everglades. *Geocarto International* 29: 228–243.

Zhang C, Xie Z, Selch D (2013) Fusing lidar and digital aerial photography for object-based forest mapping in the Florida Everglades. *GIScience & Remote Sensing* 50(5): 562–573.

Zhang C and Xie X (2012) Combining object-based texture measures with a neural network for vegetation mapping in the Everglades from hyperspectral imagery. *Remote Sensing of Environment* 124: 310–320.

Zhang, K., & Whitman, D. (2005). Comparison of Three Algorithms for Filtering Airborne LiDAR Data. *Photogrammetric Engineering & Remote Sensing*, *71*(3), 313–324. https://doi.org/10.14358/PERS.71.3.313

Zhu, G., & Blumberg, D. G. (2002). Classification using ASTER data and SVM algorithms; The case study of Beer Sheva, Israel. *Remote Sensing of Environment*, 8.